Energía magnetostática – existencia de dominios

Energía magnetostática

Energía de interación entre los dipolos de un material magnetizado

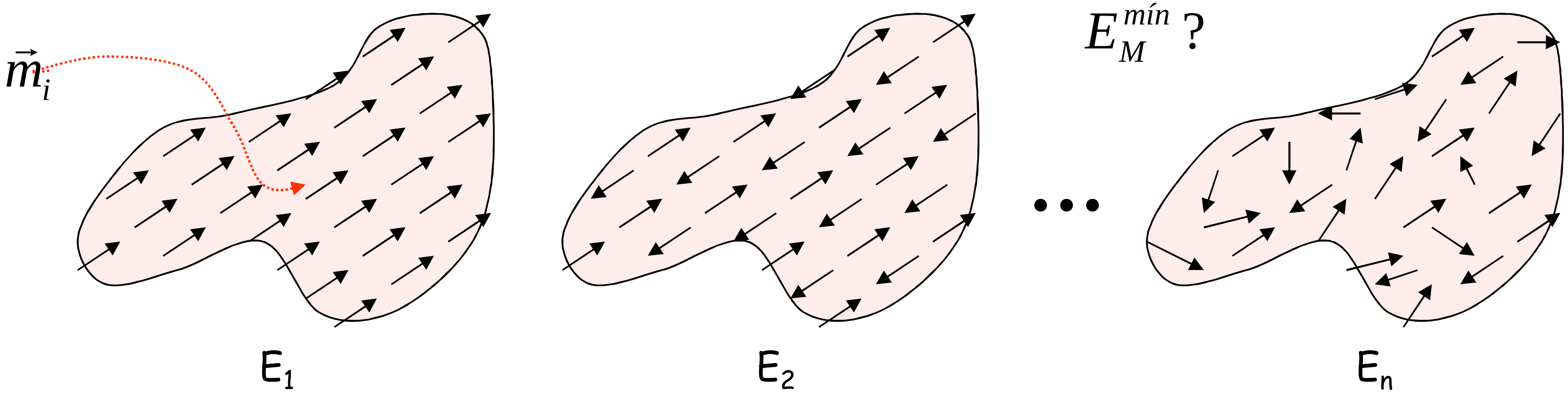

$E_M^{mín}$?

$$E_M = -\frac{1}{2}\sum_i \vec{m}_i \cdot \vec{B}_i = -\frac{\mu_0}{2}\sum_i \vec{m}_i \cdot \vec{H}_i = -\frac{\mu_0}{2}\sum_i \vec{M}_i \cdot \vec{H}_i\, V_i \approx -\frac{\mu_0}{2}\int \vec{M} \cdot \vec{H} dV$$

$$\vec{B}_i = \sum_{j \neq i} \vec{B}_j(\vec{r}_i)$$

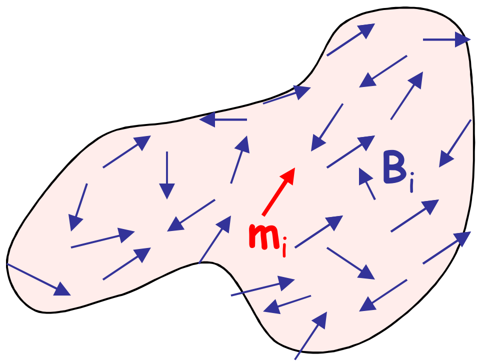

Energía magnetostática

Energía de interación entre los dipolos de un material magnetizado

Evaluación de:

$$E_M = -\frac{\mu_0}{2}\int \vec{M}\cdot\vec{H}dV$$

Dado un cuerpo (forma, volumen V, superficie S),

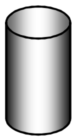

Una distribución de magnetización **M**,

y las ecuaciones de Maxwell:

$$\nabla\cdot\vec{B} = 0\,,$$
$$\nabla\times\vec{E} + \partial\vec{B}/\partial t = 0\,,$$
$$\nabla\cdot\vec{D} = \rho\,,$$
$$\nabla\times\vec{H} - \partial\vec{D}/\partial t = \vec{j}\,.$$

En ausencia de corrientes:

$$\vec{\nabla}\cdot\vec{B} = 0$$
$$\vec{\nabla}\times\vec{H} = 0$$

además

$$\begin{cases}\vec{B} = \mu_0\left(\vec{H}+\vec{M}\right)\\ \vec{H} = -\vec{\nabla}U\end{cases}$$

Potencial escalar

U continuo

$$\vec{\nabla}\cdot\left(-\vec{\nabla}U+\vec{M}\right) = 0$$

$$\nabla^2 U_{\text{int}} = \vec{\nabla}\cdot\vec{M}$$
$$\nabla^2 U_{out} = 0$$

Energía magnetostática

Energía de interación entre los dipolos de un material magnetizado

$M(\vec{r})$ dada

condiciones de contorno

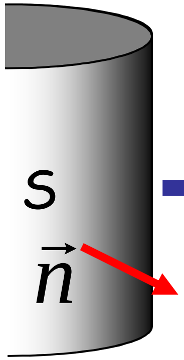

$$U_{\text{int}}\big|_S = U_{ext}\big|_S$$

$$\left.\frac{\partial U_{\text{int}}}{\partial n}\right|_S - \left.\frac{\partial U_{ext}}{\partial n}\right|_S = \vec{M}\cdot\vec{n}$$

$|rU|$

$|r^2U|$

Acotadas para $r \to \infty$

+

$$\nabla^2 U_{\text{int}} = \vec{\nabla}\cdot\vec{M}$$

$$\nabla^2 U_{ext} = 0$$

Se puede demostrar que el problema tiene solución única

$$U(\vec{r})$$

$$\vec{H} = -\vec{\nabla} U$$

$$E_M = -\frac{\mu_0}{2}\int \vec{M}\cdot\vec{H}\,dV$$

Energía magnetostática

Ejemplo: Esfera de radio R magnetizada uniformemente

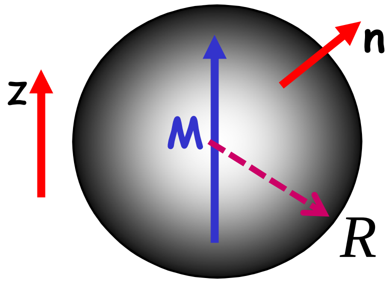

$$\vec{\nabla}\cdot\vec{M}=0$$

M uniforme

$$\nabla^2 U=\left[\frac{1}{r^2}\frac{\partial}{\partial r}r^2\frac{\partial}{\partial r}+\frac{1}{r^2\sin\theta}\frac{\partial}{\partial\theta}\sin\theta\frac{\partial}{\partial\theta}+\frac{1}{r^2\sin^2\theta}\frac{\partial^2}{\partial\phi^2}\right]U=0$$

$$\frac{\partial}{\partial n}=\frac{\partial}{\partial r}$$

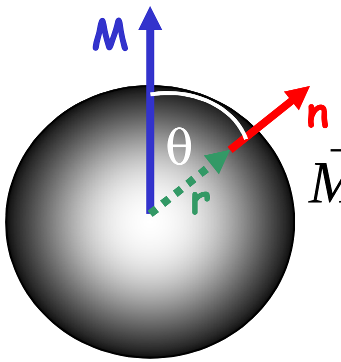

$$\vec{M}\cdot\vec{n}=M_S\cos\theta \Rightarrow \left.\frac{\partial U_{\text{int}}}{\partial r}\right|_S-\left.\frac{\partial U_{ext}}{\partial r}\right|_S=M_S\cos\theta$$

solución

$$U(\vec{r})=\frac{M_S}{3}\cos\theta\times\begin{cases} r, \text{ si } r\le R & U(\vec{r})=\dfrac{M_S z}{3} \\ \dfrac{R^3}{r^2} \text{ si } r>R & U(\vec{r})=\dfrac{M_S z}{3}\left(\dfrac{R}{r}\right)^3 \end{cases}$$

Energía magnetostática

$$U(\vec{r}) = \frac{M_S}{3}\cos\theta \times \begin{cases} r, \text{ si } r \le R \\ \dfrac{R^3}{r^2} \text{ si } r > R \end{cases}$$

$$\begin{cases} U_{\text{int}} = \dfrac{M_S}{3} z \\ \vec{H}_{\text{int}} = -\vec{\nabla} U_{\text{int}} \end{cases}$$

$$\begin{cases} H_{\text{int}_x} = H_{\text{int}_y} = 0 \\ H_{\text{int}_z} = -\dfrac{M_S}{3} \end{cases}$$

$$U_{ext} = \frac{M_S R^3 \cos\theta}{3r^2} = \frac{M_S R^3 z}{3\left(x^2 + y^2 + z^2\right)^{3/2}}$$

$$H_{ext_x} = \frac{M_S R^3 xz}{r^5}$$

$$H_{ext_y} = \frac{M_S R^3 yz}{r^5}$$

$$H_{ext_z} = \frac{M_S R^3}{r^3}\left(\frac{z^2}{r^2} - \frac{1}{3}\right)$$

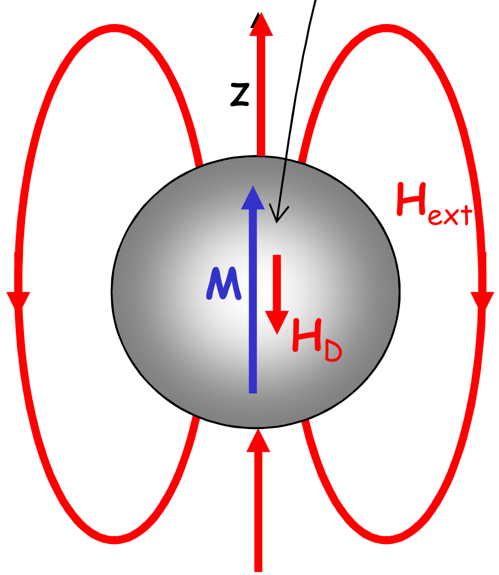

Energía magnetostática

Esfera magnetizada uniformemente

energía

$$E_M = -\frac{\mu_0}{2}\int \vec{M}\cdot\vec{H}dV = -\frac{\mu_0}{2}M_S H_{\text{int}_z} V_{esfera} = \frac{\mu_0}{2}M_S \frac{M_S}{3}\frac{4\pi R^3}{3} = \frac{2\pi R^3 \mu_0 M_S^2}{9}$$

$$H_{\text{int}_z} = -\frac{M_S}{3}$$

$$E_M = \frac{2\pi R^3 \mu_0 M_S^2}{9}$$

generalizando para otras geometrías

Factor demagnetizante

$$H_{\text{int}_z} = -N_D M_S$$

generalizando para otras geometrías y distribuciones de la magnetización

$$E_M = C\mu_0 M_S^2$$

Esfera

si

$$\vec{M} = M_S\breve{x} \Rightarrow N_x = 1/3$$

$$\vec{M} = M_S\breve{y} \Rightarrow N_y = 1/3$$

$$\vec{M} = M_S\breve{z} \Rightarrow N_z = 1/3$$

$$N_x + N_y + N_z = 1$$

Energía magnetostática

Cilindro infinito magnetizado uniformemente en dirección perpendicular al eje

$$\nabla^2 U = \vec{\nabla} \cdot \vec{M}$$

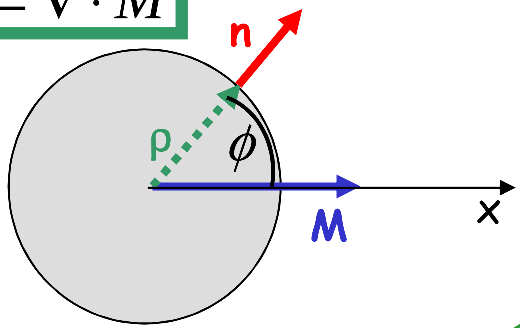

$$\vec{\nabla} \cdot \vec{M} = 0 \Rightarrow \nabla^2 U = 0$$

$$\frac{\partial}{\partial n} = \frac{\partial}{\partial \rho}$$

$$\left.\frac{\partial U_{\text{int}}}{\partial n}\right|_S - \left.\frac{\partial U_{ext}}{\partial n}\right|_S = \vec{M} \cdot \vec{n}$$

$$\vec{M} \cdot \vec{n} = M_S \cos\phi$$

$$\left(\frac{1}{\rho}\frac{\partial}{\partial \rho}\rho\frac{\partial}{\partial \rho} + \frac{1}{\rho^2}\frac{\partial^2}{\partial \phi^2} + \frac{\partial^2}{\partial z^2} \right) U = 0$$

$$\left.\frac{\partial U_{\text{int}}}{\partial \rho}\right|_S - \left.\frac{\partial U_{ext}}{\partial \rho}\right|_S = M_S \cos\phi$$

$$U = \frac{M_S}{2}\cos\phi \times \begin{cases} \rho, \text{ si } \rho \le R \\ \dfrac{R^2}{\rho} \text{ si } \rho > R \end{cases}$$

$$\begin{cases} H_{\text{int}_z} = H_{\text{int}_y} = 0 \\ H_{\text{int}_x} = -\dfrac{M_S}{2} \end{cases}$$

Energía magnetostática

Cilindro infinito magnetizado uniformemente en dirección perpendicular a su eje

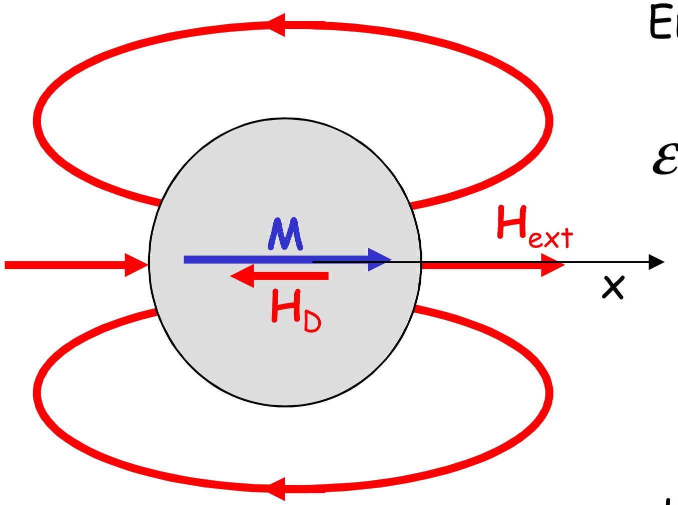

Energía magnetostática por unidad de área ⊥ al eje del cilindro

$$\varepsilon_M = -\frac{\mu_0}{2}\int \vec{M}\cdot\vec{H}dS = -\frac{\mu_0}{2}M_S\frac{M_S}{2}\pi R^2 = \frac{\pi R^2\mu_0 M_S^2}{4}$$

$$H_{\text{int}_x} = -\frac{M_S}{2}$$

$$\varepsilon_M = \frac{\pi R^2\mu_0 M_S^2}{4}$$

de la forma

de la forma

Factor demagnetizante

$$H_{\text{int}_z} = -N_D M_S$$

$$\varepsilon_M = C\mu_0 M_S^2$$

$$\vec{M} = M_S\breve{x} \Rightarrow N_x = 1/2$$

$$\vec{M} = M_S\breve{y} \Rightarrow N_y = 1/2$$

$$\vec{M} = M_S\breve{z} \Rightarrow N_z = 0$$

$$N_x + N_y + N_z = 1$$

Energía magnetostática

Otros cuerpos magnetizados uniformemente

M uniforme → Caso general → $\mathbf{H}_{int}$ NO uniforme

M uniforme → Superficie de 2do grado (cónicas) → $\mathbf{H}_{int}$ uniforme

elipsoide

$$\left(\frac{x}{a}\right)^2 + \left(\frac{y}{b}\right)^2 + \left(\frac{z}{c}\right)^2 = 1 \;\longrightarrow\; \vec{H}_D = -\hat{N}\vec{M}$$

M uniforme

$\vec{H}_D$: Campo demagnetizante

$\hat{N}$: Tensor demagnetizante

Tensor demagnetizante → Diagonal si los ejes de coordenadas coinciden con los del elipsoide

Tensor demagnetizante → Traza unitaria

$$N_x + N_y + N_z = 1$$

Tensor demagnetizante → Número si además

$$\vec{M} = \begin{cases} M_S\vec{i} \\ M_S\vec{j} \\ M_S\vec{k} \end{cases}$$

Energía magnetostática

elipsoides

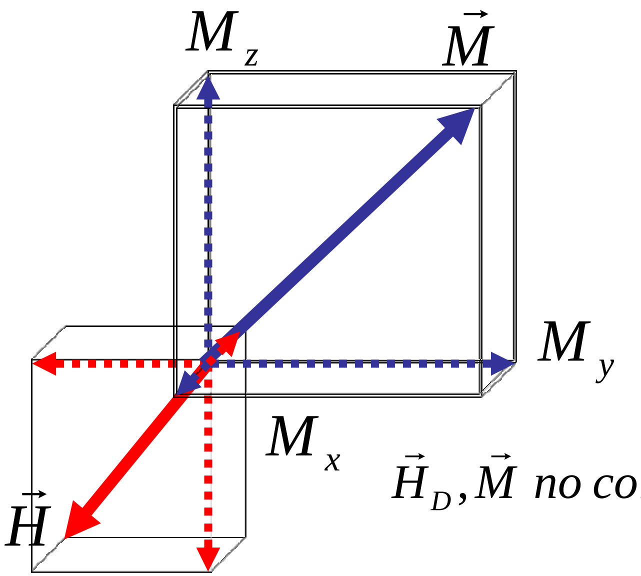

$\vec{H}_D, \vec{M}$ *no colineales*

$$\vec{H}_D = -\hat{N}\vec{M} \Rightarrow \begin{cases} H_x = -N_x M_x \\ H_y = -N_y M_y \\ H_z = -N_z M_z \end{cases}$$

$$N_x + N_y + N_z = 1$$

$$M_i, H_i, unif.$$

$$E_M = -\frac{\mu_0}{2}\int \vec{M}\cdot\vec{H}dV = -\frac{\mu_0}{2}\left(M_x H_x + M_y H_y + M_z H_z\right)V$$

$$E_M = \frac{\mu_0}{2}\left(N_x M_x^2 + N_y M_y^2 + N_z M_z^2\right)V$$

Energía magnetostática

Elipsoide prolado u oblado

$$a = b < c \Rightarrow N_x = N_y > N_z$$

$$a = b > c \Rightarrow N_x = N_y < N_z$$

prolado

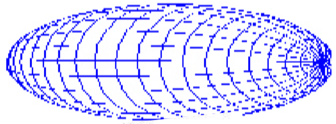

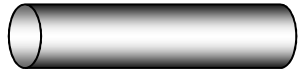

oblado

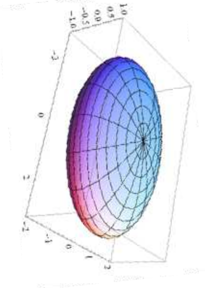

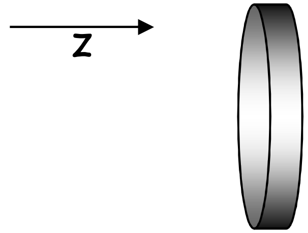

$$N_x = N_y$$

$$E_M = \frac{\mu_0 V}{2}\left(N_x M_x^2 + N_y M_y^2 + N_z M_z^2\right) = \frac{\mu_0 V}{2}\left(N_x\left(M_x^2 + M_y^2\right) + N_z M_z^2\right)$$

$$M_x^2 + M_y^2 = M_S^2 - M_z^2$$

$$E_M = \frac{\mu_0 V}{2}(N_z - N_x)M_z^2 + cte = \frac{\mu_0 V}{2}(N_z - N_x)M_S^2 \cos^2\theta + cte$$

$$E_M = -\frac{\mu_0 V}{2}(N_z - N_x)M_S^2 \sin^2\theta + cte = K_S \sin^2\theta + cte$$

$$\boxed{E_M = K_S V \sin^2\theta}$$

$$\boxed{K_S = \frac{\mu_0}{2}(N_x - N_z)M_S^2}$$

Energía magnetostática

Elipsoide de revolución prolado

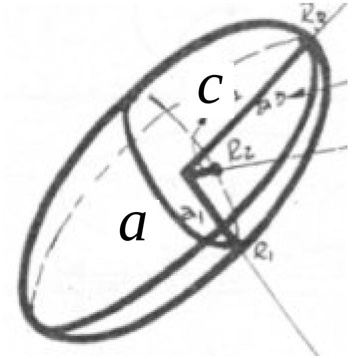

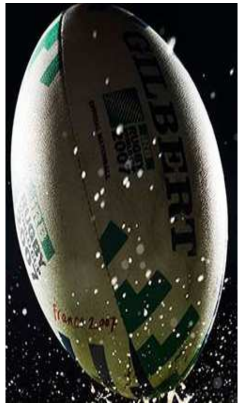

$$p = c/a$$

$$\xi = \left(\sqrt{p^2 - 1}\right)/\, p$$

Puede demostrarse que

$$N_z = \frac{1}{p^2 - 1}\left[\frac{1}{2\xi}\ln\left(\frac{1+\xi}{1-\xi}\right) - 1\right]$$

$$c \rightarrow a$$

$$N_z = \frac{1}{p^2}\left[\frac{1}{3} + \sum_{k=1}^{\infty}\frac{1}{2k+3}\left(\frac{p^2-1}{p^2}\right)^k\right] \xrightarrow[p \to 1]{} \frac{1}{3} \Rightarrow N_z^{esfera} = \frac{1}{3}$$

esfera $\quad N_x = N_y = \dfrac{1 - N_z}{2} = \dfrac{1}{3}$

Energía magnetostática - Origen de los dominios

Cilindro infinito con dos dominios perpendiculares a su eje

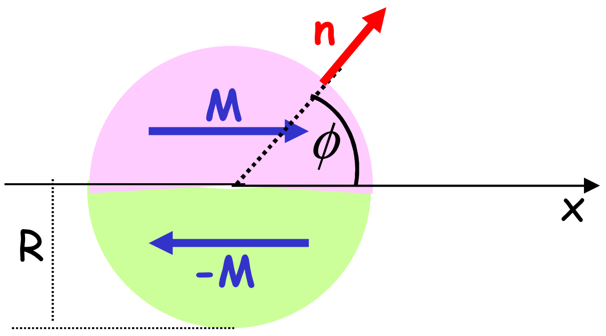

$$M_y = M_z = 0$$

$$M_x = M_S \times \begin{cases} +1 \leftrightarrow 0 \le \phi < \pi \\ -1 \leftrightarrow \pi \le \phi < 2\pi \end{cases}$$

Desarrollo en serie de Fourier de la función de Heaviside

$$M_x = \frac{4M_S}{\pi} \sum_{n=0}^{\infty} \frac{\sin(2n+1)\phi}{2n+1}$$

$$M_n = M_x \cos\phi = \frac{4M_S}{\pi} \sum_{n=0}^{\infty} \frac{\sin(2n+1)\phi}{2n+1} \cos\phi$$

$$M_n = \frac{2M_S}{\pi} \sum_{n=0}^{\infty} \frac{\sin(2n+2)\phi + \sin(2n\phi)}{2n+1}$$

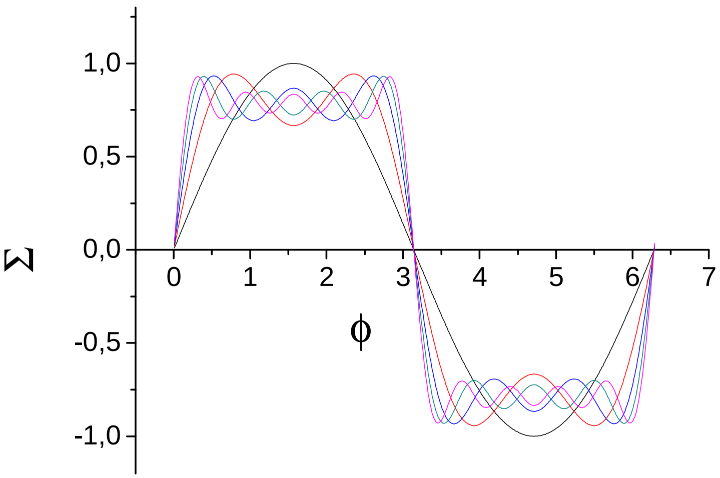

Energía magnetostática - Origen de los dominios

Cilindro infinito con dos dominios perpendiculares a su eje

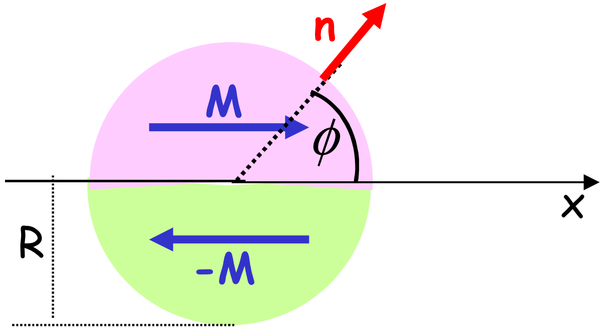

$$M_n = \frac{2M_S}{\pi}\sum_{n=0}^{\infty}\frac{\sin(2n+2)\phi+\sin(2n\phi)}{2n+1}$$

$$\left.\frac{\partial U_{\text{int}}}{\partial n}\right|_S - \left.\frac{\partial U_{ext}}{\partial n}\right|_S = \vec{M}\cdot\vec{n} = M_n$$

$$\left(\frac{\partial U_{\text{int}}}{\partial \rho}-\frac{\partial U_{ext}}{\partial \rho}\right)_{\rho=R} = \frac{8M_S}{\pi}\sum_{n=1}^{\infty}\frac{n\sin(2n\phi)}{(2n+1)(2n-1)} \oplus \nabla^2 U = 0$$

$$U = \sum_{n=1}^{\infty} u_n(\rho)\sin(2n\phi)$$

$$u_n(\rho) = c_n \times \begin{cases}(\rho/R)^{2n} \leftrightarrow \rho \le R \\ (R/\rho)^{2n} \leftrightarrow \rho \ge R\end{cases}$$

$$U_{\text{int}} = \frac{2RM_S}{\pi}\sum_{n=1}^{\infty}\frac{\sin(2n\phi)}{(2n+1)(2n-1)}\left(\frac{\rho}{R}\right)^{2n}$$

Energía magnetostática - Origen de los dominios

Cilindro infinito con dos dominios perpendiculares a su eje

$$U_{\text{int}} = \frac{2RM_S}{\pi}\sum_{n=1}^{\infty}\frac{\sin(2n\phi)}{(2n+1)(2n-1)}\left(\frac{\rho}{R}\right)^{2n}$$

$$\vec{H}_{\text{int}} = -\vec{\nabla} U_{\text{int}}$$

$$\Rightarrow \begin{cases} H_{\text{int}_z} = H_{\text{int}_y} = 0 \\ H_{\text{int}_x} = -\dfrac{4M_S}{\pi}\displaystyle\sum_{n=1}^{\infty}\frac{n\sin(2n-1)\phi}{(2n+1)(2n-1)}\left(\frac{\rho}{R}\right)^{2n-1} \end{cases}$$

Energía magnetostática por unidad de área ⊥ al eje del cilindro

$$\varepsilon_M = -\frac{\mu_0}{2}\int \vec{M}\cdot\vec{H}\,dS = -\frac{\mu_0}{2}\int M_x H_x\,dS = \frac{R^2}{\pi}\mu_0 M_S^2$$

1 dominio

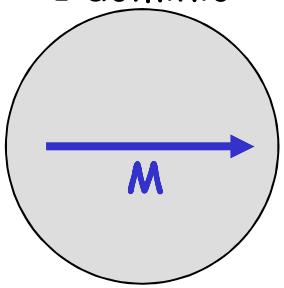

2 dominios

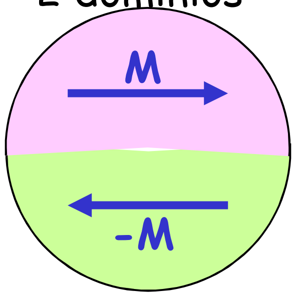

$$\varepsilon_M^{(1)} = \frac{\pi R^2 \mu_0 M_S^2}{4} \qquad \varepsilon_M^{(2)} = \frac{R^2}{\pi}\mu_0 M_S^2$$

$$\frac{E_M^{(2)}}{E_M^{(1)}} = \frac{4}{\pi^2} \approx 0.41 < \frac{1}{2} \Rightarrow \frac{E_M^{(n)}}{E_M^{(1)}} \approx \frac{1}{n}$$

Regla aproximada

Energía magnetostática - Origen de los dominios

monodominio

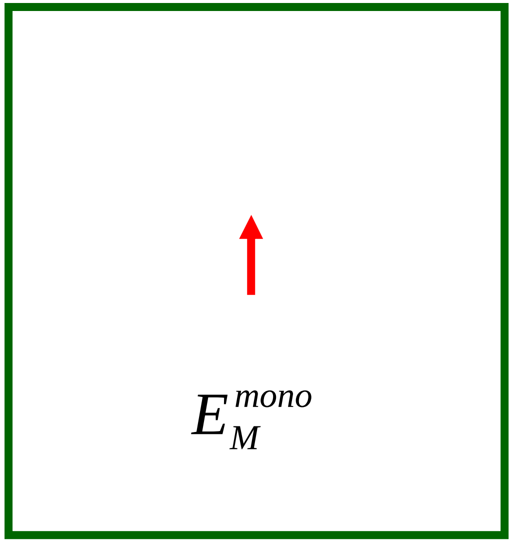

multidominio

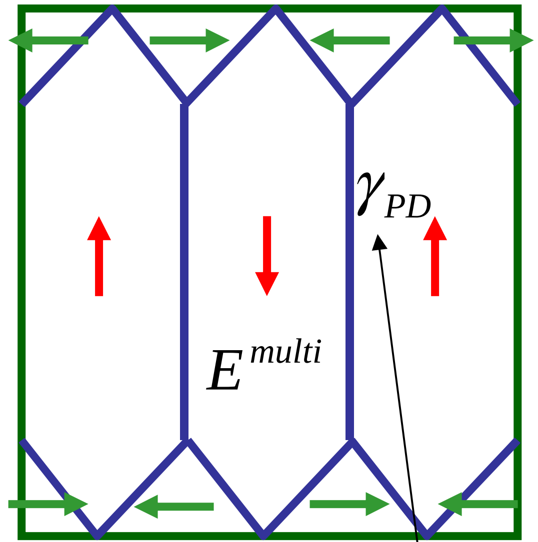

Energía de pared por unidad de área

$$E^{multi} \approx \frac{E_M^{mono}}{n} + S_{int}(n)\gamma_{PD}$$

E magnetostática decrece

E pared dominios crece

Nro dominios en equilibrio

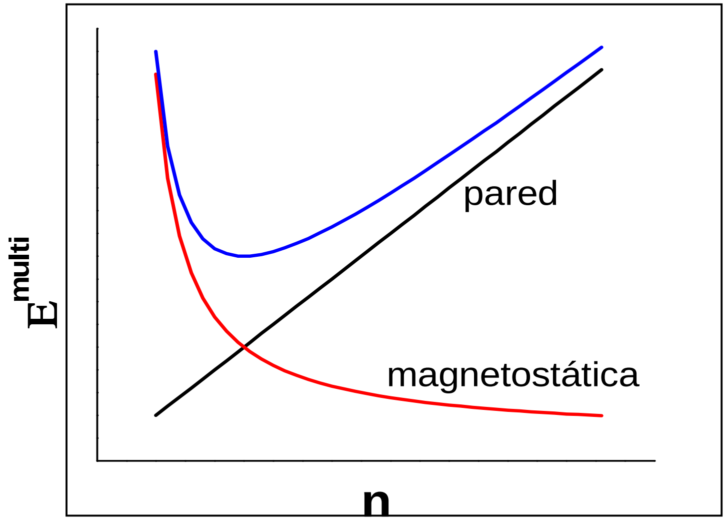

Energía magnetostática - Origen de los dominios

Superficies no cuadráticas

$$E_M = \frac{\mu_0 V}{2}\left(N_x M_x^2 + N_y M_y^2 + N_z M_z^2\right)$$

Válido también para cuerpos con superficies no cuadráticas: cubos, prismas, cilindros, octaedros, etc.

(teorema de Brown-Morrish)

Casos particulares

Cubo, octaaedro, tetraedro

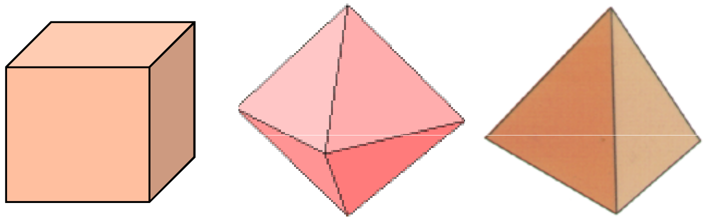

$$N_x = N_y = N_z = 1/3$$

Prisma regular, cilindro

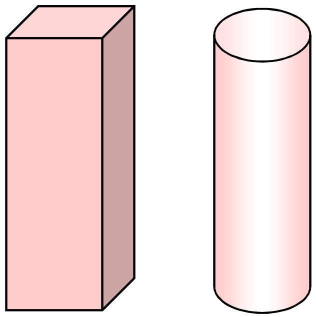

$$N_x = N_y \neq N_z$$

Energía magnetostática - campo efectivo

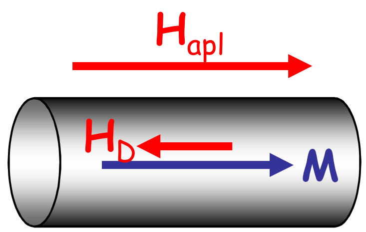

$$\vec{H}_D = -N\vec{M}$$

$$\vec{H}_{ef} = \vec{H}_{apl} + \vec{H}_D = \vec{H}_{apl} - N\vec{M}$$

Cuando se grafica M vs. H debe usarse como abscisa el H_{ef}

$$H_{apl} \Rightarrow M \Rightarrow H_{ef}$$

Si $M \ll M_S$ ⇨ $\vec{M} = \chi\vec{H}_{ef}$

$$\vec{H}_{ef} = \vec{H}_{apl} - N\chi\vec{H}_{ef} \quad ⇨ \quad \vec{H}_{ef} = \frac{\vec{H}_{apl}}{1+N\chi} \quad ⇨ \quad \vec{M} = \frac{\chi}{1+N\chi}\vec{H}_{apl}$$

Si $M = M_S$

$$H_{ef} = H_{apl} - NM_S$$

Ejemplo, Ni

$$M_S \approx 4.8x10^5 A/m \approx 0.6 Tesla$$ ⇨ H_D puede alcanzar valores considerables dependiendo de la forma de la muestra

Energía magnetostática – factores demagnetizantes

Cálculos para elipsoides

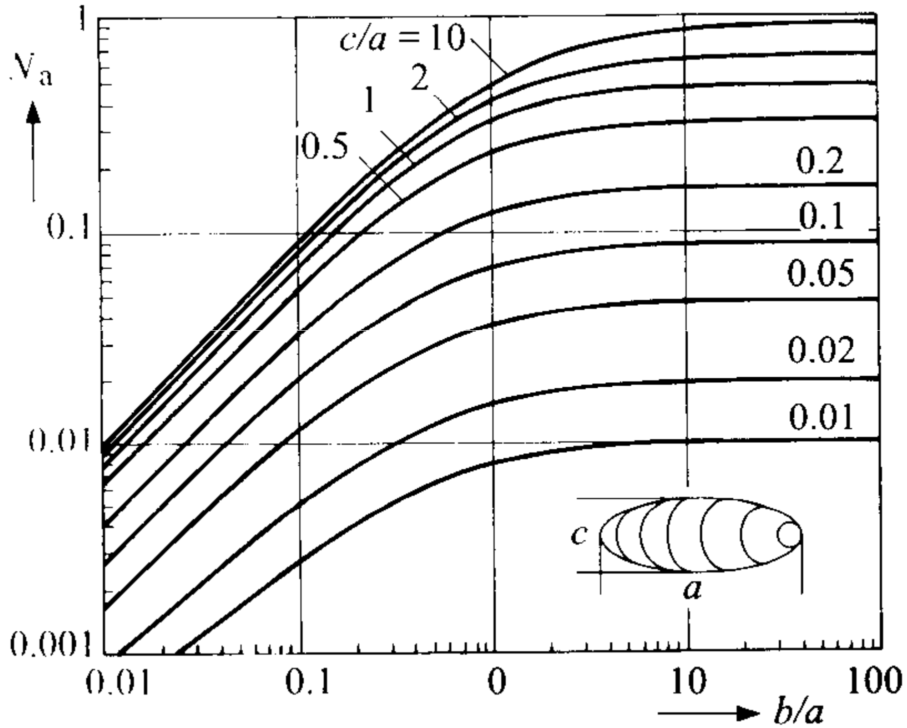

a)

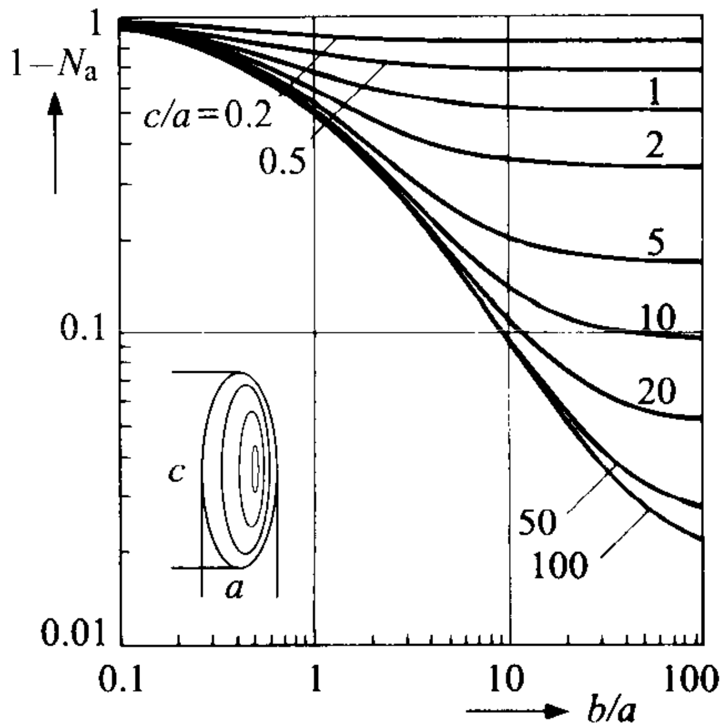

b)

Energía magnetostática – factores demagnetizantes

Cálculos en prismas

Demagnetizing factors for rectangular ferromagnetic prisms

Amikam Aharoni[a)]
Department of Electronics, Weizmann Institute of Science, 76100 Rehovoth, Israel
JOURNAL OF APPLIED PHYSICS
VOLUME 83, NUMBER 6
15 MARCH 1998

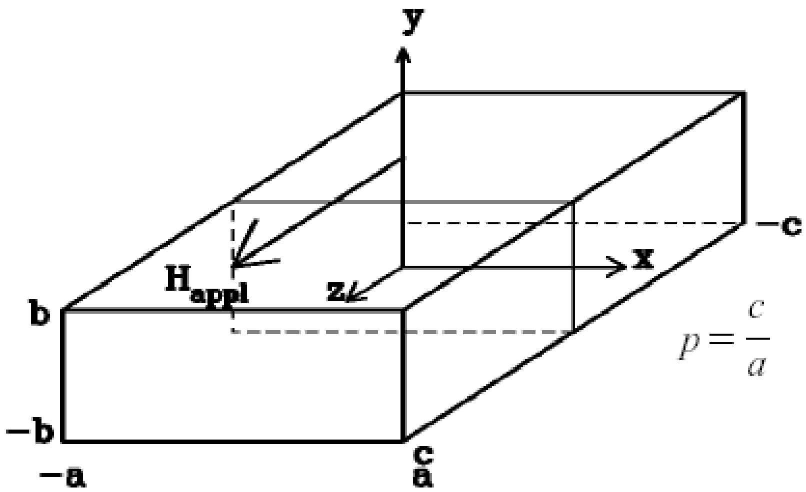

TABLE I. The demagnetizing factor, D_z^s, of a prolate spheroid and the magnetometric demagnetizing factor, D_z^p, of a square prism, for an aspect ratio, p.

p	D_z^s	D_z^p
2.0	0.17356	0.19832
3.0	0.10871	0.14036
4.0	0.075407	0.10845
5.0	0.055821	0.088316
6.0	0.043230	0.074466
7.0	0.034609	0.064363
8.0	0.028421	0.056670
9.0	0.023816	0.050617
10.0	0.020286	0.045731
11.0	0.017515	0.041705

FIG. 1. The coordinate system used in the calculations. Its origin is at the center of the rectangular prism. The field H_{appl} is applied along the z axis.

Energía magnetostática – referencias

Fórmulas, tablas y gráficos de factores demagnetizantes, Chen et al. IEEE Trans. Magnetics **27**, 3601-19 (1991)

Campo demagnetizante y medidas magnéticas, J.A. Brug y W.P. Wolf, J.Appl.Phys. **57**, 4685-701 (1985)

Cálculo de factores demagnetizantes, http://magnet.atp.tuwien.ac.at/dittrich/?http://magnet.atp.tuwien.ac.at/dittrich/content/tools/magnetostatics/streufeld.htm

Dominios y paredes de dominio

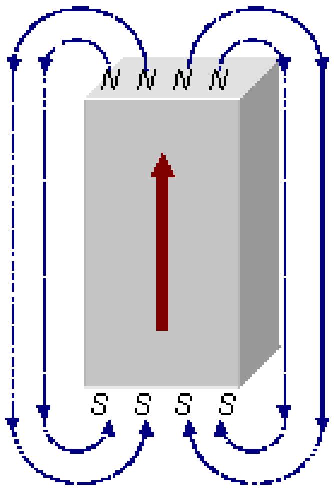

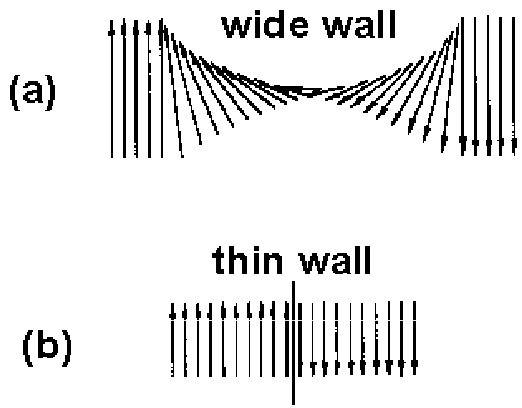

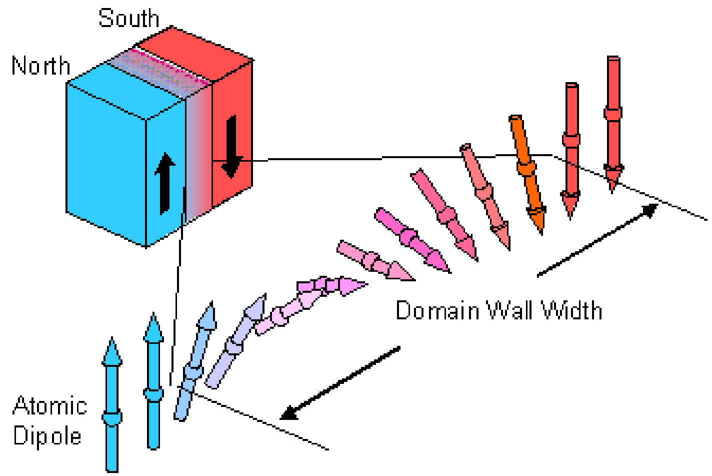

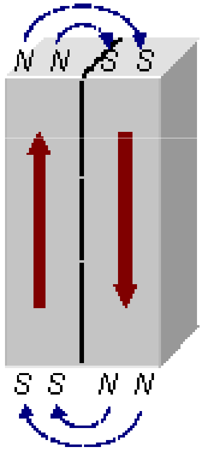

MFM

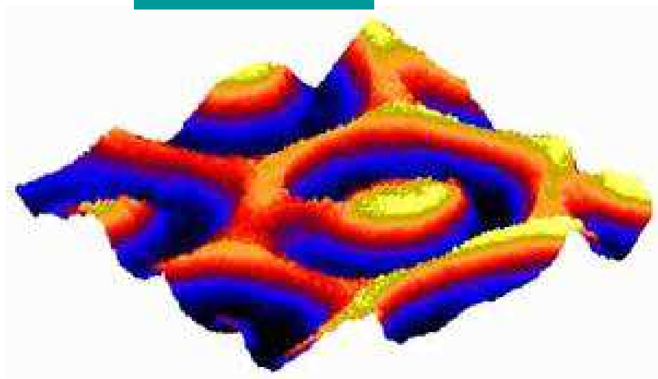

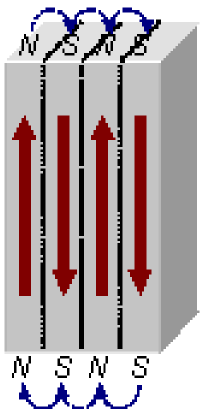

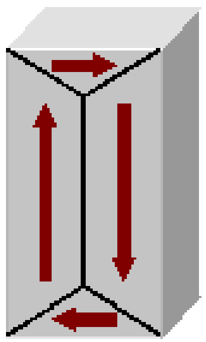

Pseudo-3d MFM image of a $(YSmLaCa)_3$ $(FeGe)_5$ O_{12} magnetic thin film garnet, 4.5 x 4.5 μm^2, domain walls appear dark;

Pared de Bloch de 180°

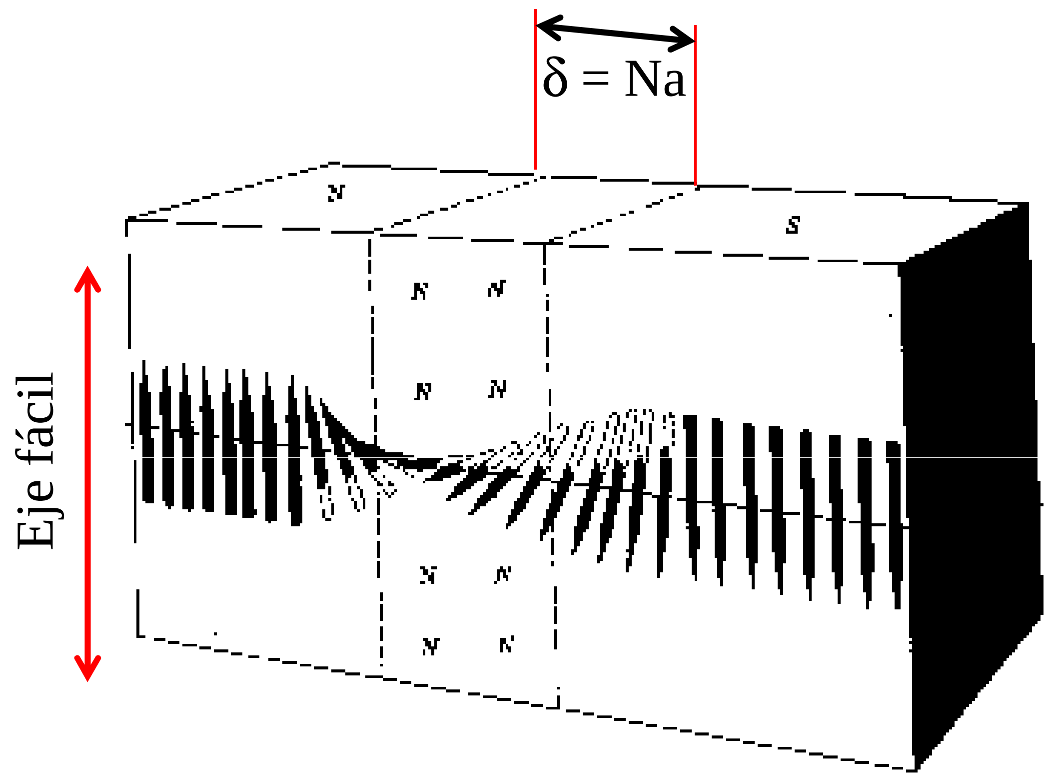

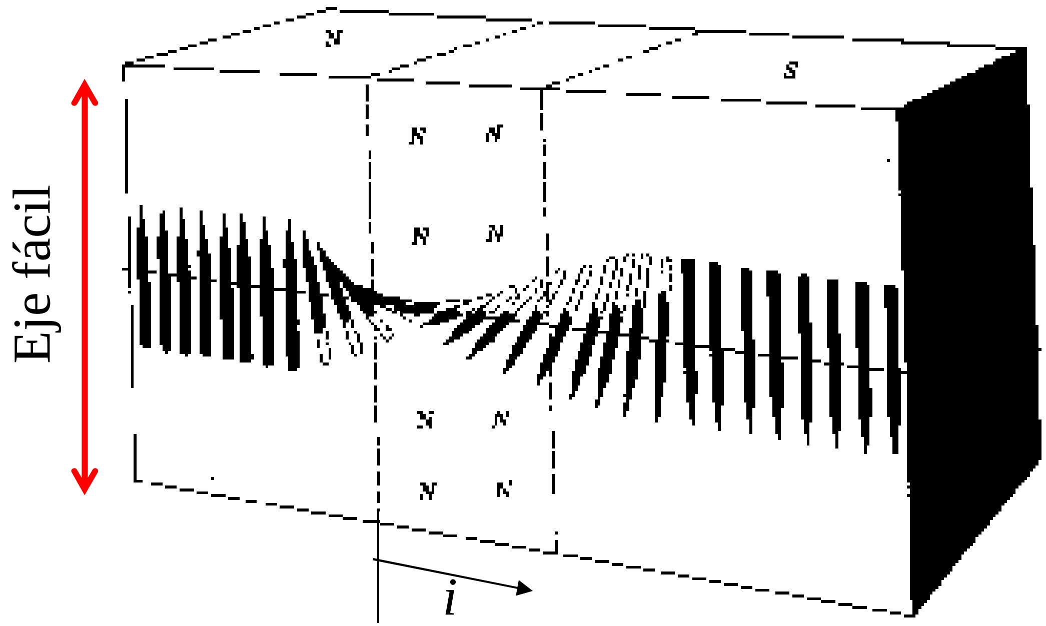

Balance energético entre anisotropía e intercambio

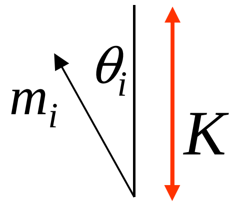

Anisotropía uniaxial

$$E_K = a^3 \sum_1^N K sen^2 \theta_i$$

Para un prisma de N celdas (base a^2)
a: parámetro de la celda cúbica

$$\theta_i = \pi i / N$$

$$\Delta i = \frac{N \Delta \theta_i}{\pi} = 1$$

$$E_K = a^3 \sum_i K sen^2 \theta_i \Delta i$$

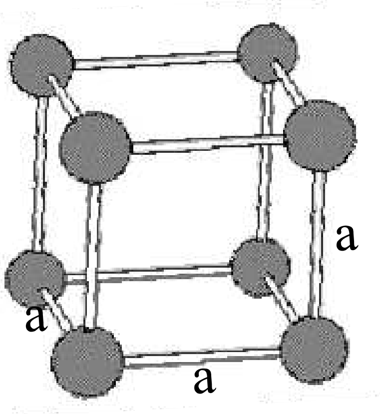

$$E_K = \frac{K N a^3}{\pi} \sum_i sen^2 \theta_i \Delta \theta \approx \frac{K N a^3}{\pi} \int_0^{\pi} sen^2 \theta_i d\theta = \frac{K N a^3}{2}$$

Por unidad de área de pared: $\varepsilon_K \approx \frac{K N a}{2}$

intercambio

$$E_J = -2NJs^2 \cos\Delta\theta = -2NJs^2 \cos(\pi/N), \quad \pi/N << 1$$

$\Delta\theta = \pi/N$

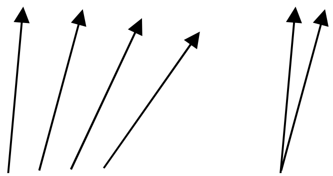

$$E_J = -2NJs^2 (1 - \frac{\pi^2}{2N^2})$$

$$\varepsilon_J = -\frac{2NJs^2}{a^2}(1 - \frac{\pi^2}{2N^2})$$

Energía de intercambio por unidad de área de pared:

Relativa al estdo fundamental:

$$\boxed{\varepsilon_J = -\frac{2NJs^2}{a^2}} \Rightarrow \Delta\varepsilon_J = \frac{\pi^2 Js^2}{Na^2}$$

Energía por unidad de área de pared

$$\gamma = \Delta\varepsilon_K + \Delta\varepsilon_J = \frac{KNa}{2} + \frac{\pi^2 Js^2}{Na^2}$$

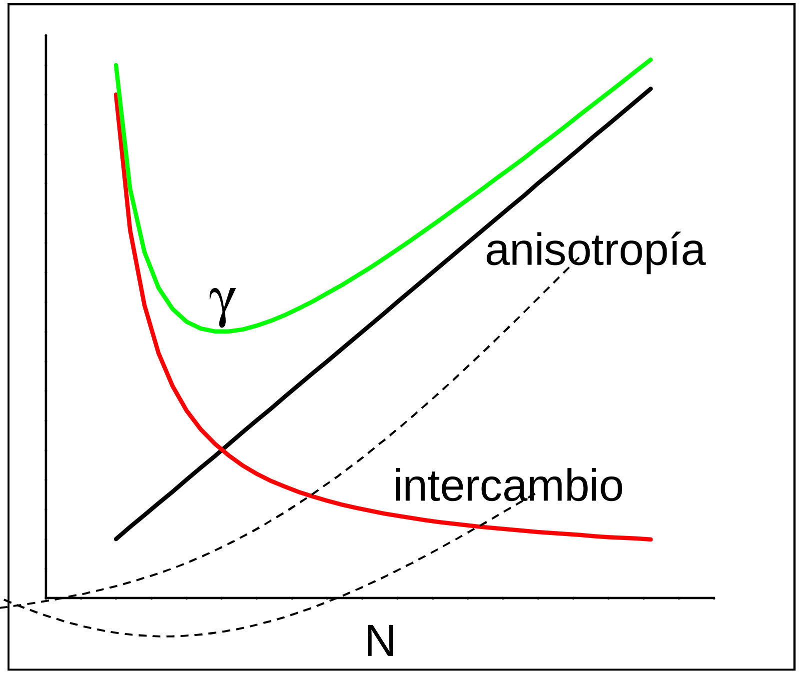

Optimización energía por unidad de área de pared

$$\gamma = \Delta\varepsilon_K + \Delta\varepsilon_J = \frac{KNa}{2} + \frac{\pi^2 Js^2}{Na^2}$$

$$d\gamma / dN = \frac{Ka}{2} - \frac{\pi^2 Js^2}{N^2 a^2} = 0$$

⇓

$$N_{eq} = \pi \left(\frac{2Js^2}{Ka^3} \right)^{1/2}$$

Ancho de la pared

$$\delta_{eq} = N_{eq} a = \pi \sqrt{\frac{2Js^2}{Ka}} = \pi \sqrt{\frac{2A}{K}}$$

$$A \approx Js^2 / a$$

Cte de stiffness

$$\gamma_{eq} = 2\pi \sqrt{2KA}$$

$$10^{-12}\ J/m \le A \le 10^{-11}\ J/m$$

$$10^3\ J/m^3 \le K \le 10^6\ J/m^3$$

$$A = 10^{-11}\ J/m$$

$$K = 10^3\ J/m^3 \Rightarrow \delta_{eq} = 444\ nm$$

$$K = 10^5\ J/m^3 \Rightarrow \delta_{eq} = 44.4\ nm$$

Observación de dominios

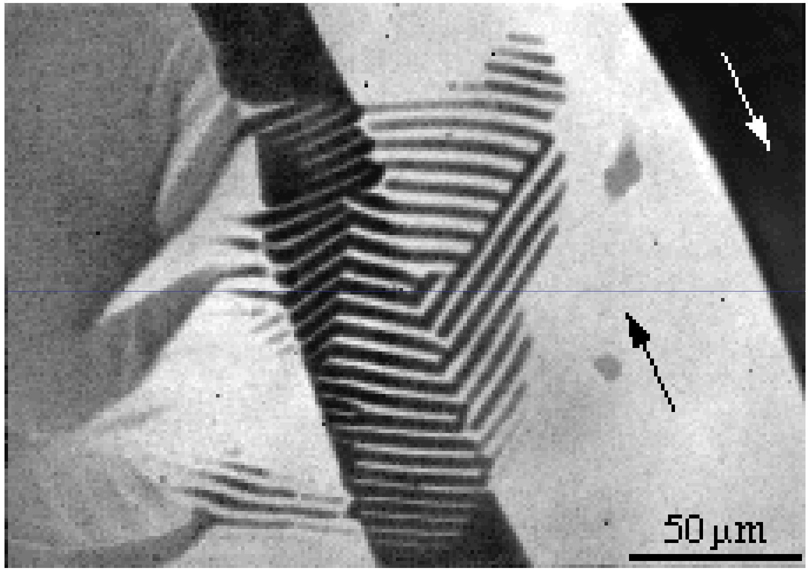

Cinta amorfa Ferromagnética

http://www.ifw-dresden.de/~schaefer/ToCBilder/5.4.htm

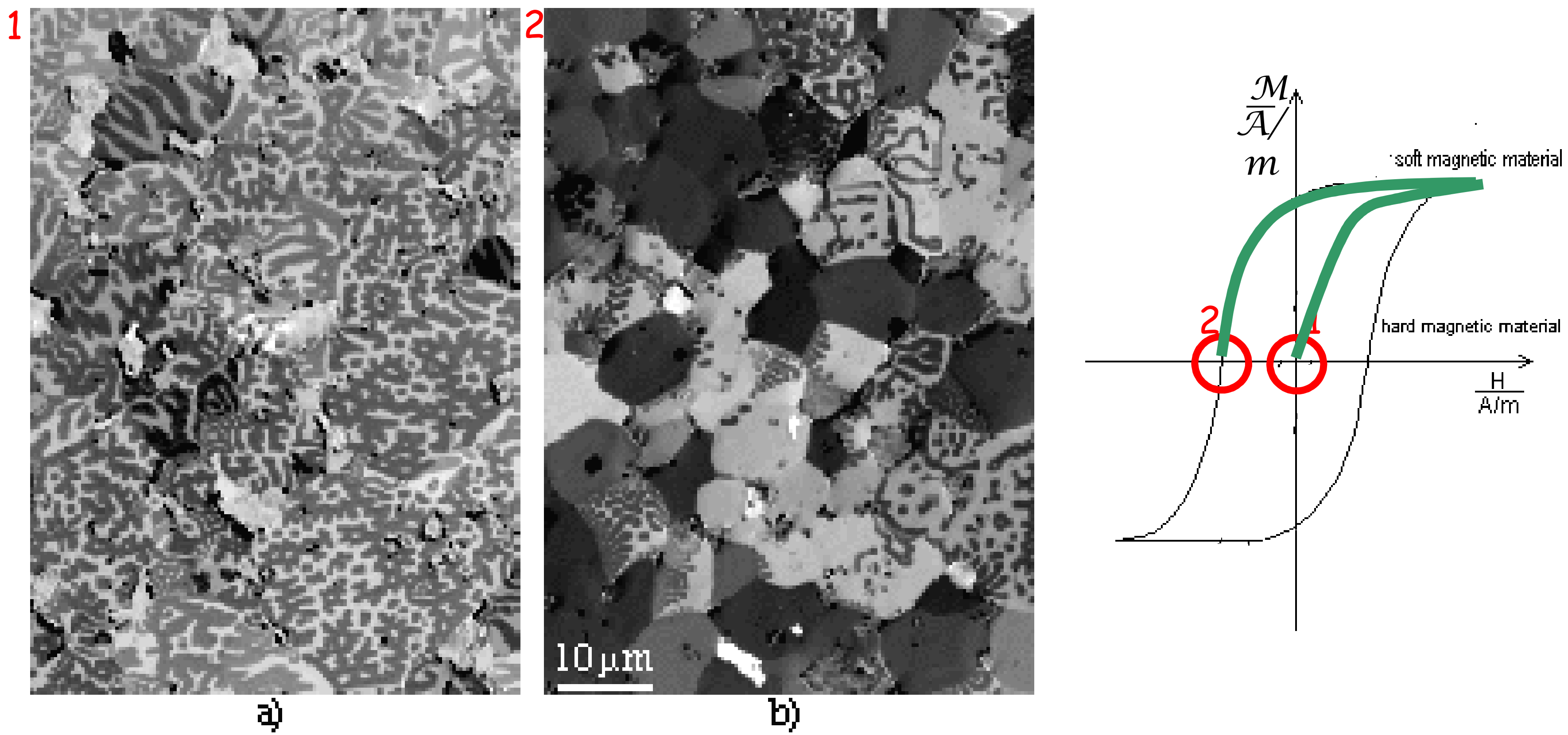

Fig. 6.19a,b: The demagnetized state of sintered NdFeB permanent magnet material depends strongly on magnetic history. (a) shows the thermally demagnetized state in which virtually all grains are demagnetized within themselves. The demagnetized state (b) was achieved by applying a field slightly higher than coercivity after saturation. Here only the average magnetization is zero, while most grains are saturated in either direction

http://www.ifw-dresden.de/~schaefer/ToCBilder/6.3.htm

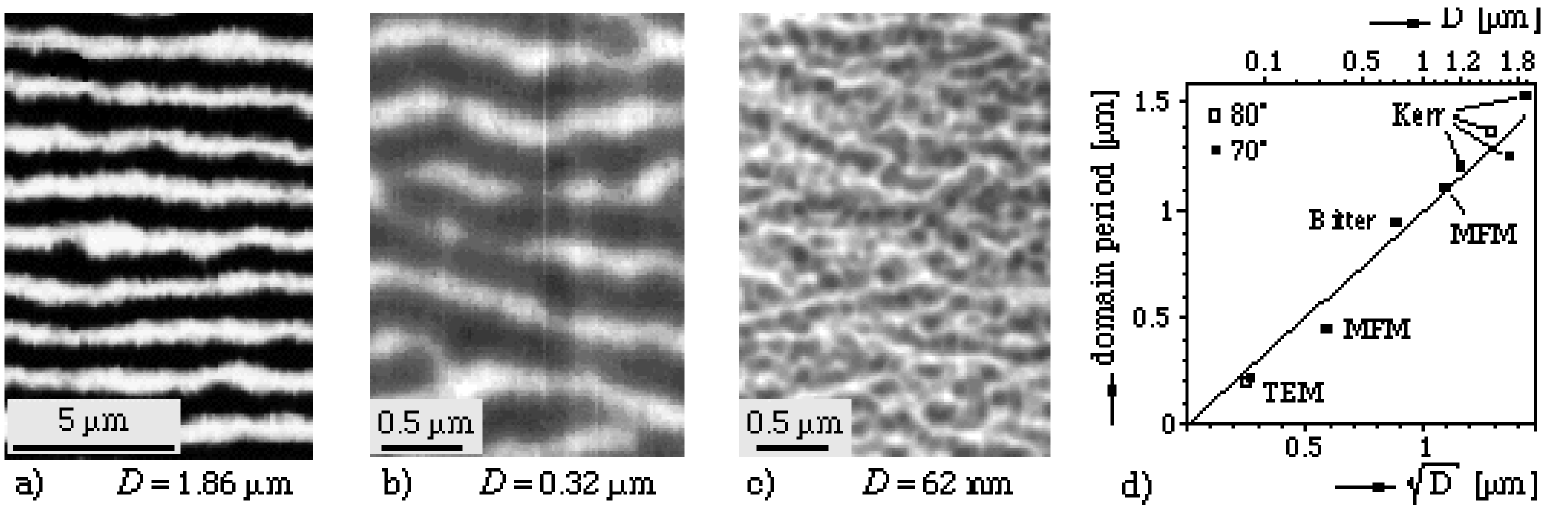

Cinta para grabación

http://www.ifw-dresden.de/~schaefer/ToCBilder/6.4.gif

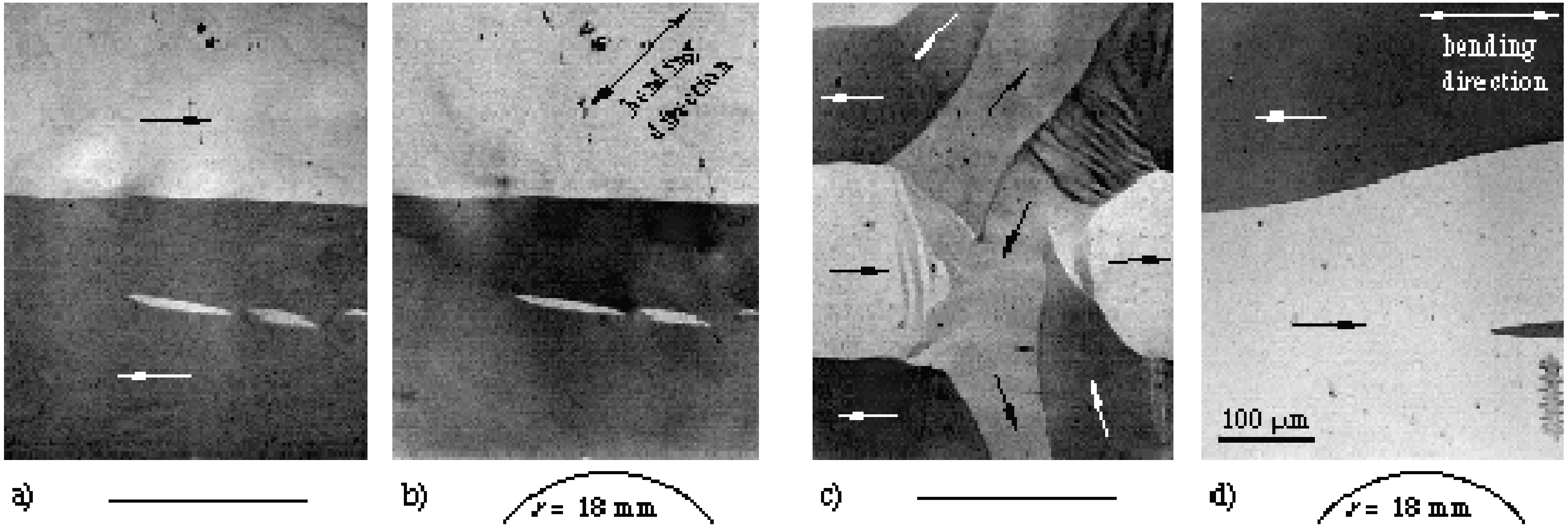

Fig. 6.13: Magnetostriction-free metallic glasses are unique soft magnetic materials in being insensitive to elastic deformation. The same domain pattern is observed in the flat state (a) and in a strongly bent state (b). In contrast, regular magnetostrictive materials display a complete domain rearrangement on bending (c, d)

http://www.ifw-dresden.de/~schaefer/ToCBilder/6.2.htm

Técnica Bitter

Técnica Bitter (1931): dispersión sobre la muestra de un líquido portador de pequeñas partículas ferromagnéticas. Las partículas se acumulan en zonas de equilibrio. Experimentan fuerzas máximas donde el gradiente de campo es máximo (bordes de dominio). Soluciones coloidales de Fe_3O_4.

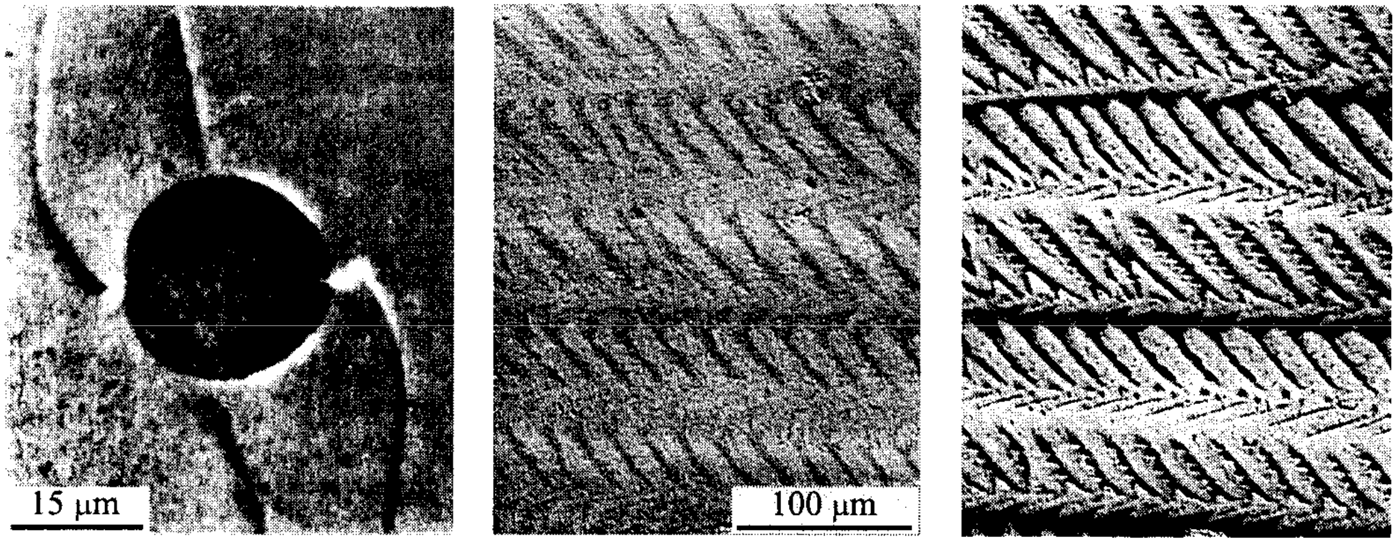

a) b) c)

Fig. 2.1 (a) Domains in an ion-implanted garnet layer made visible by Ferrofluid® (courtesy *D.B. Dove*, IBM Yorktown Heights [54]). The circular shape is unimplanted. (b, c) Stress-induced domains on a $Ni_{55}Fe_{45}$ crystal revealed by Lignosite FML®. A perpendicular field of 1.5 kA/m was applied in (c) to improve the contrast of the same pattern. The NiFe crystal has ⟨100⟩ easy directions and a near (100) surface

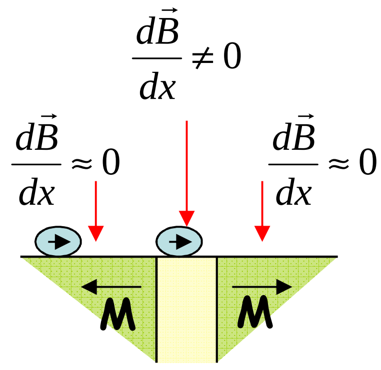

$$\vec{F} = -\vec{\nabla}E = -\vec{\nabla}\left(-\vec{m}\cdot B\right) = m\cdot\frac{dB}{dx}\breve{x}$$

Técnica Bitter

microscopía

bitter

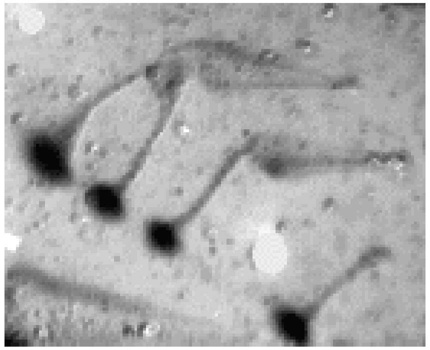

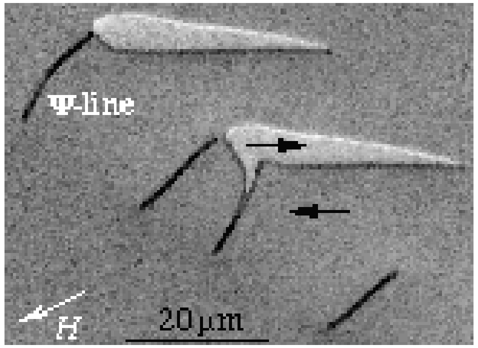

kerr

patrones de dominio en láminas (110) ligeramente desorientadas de silicio-hierro (c). Los patrones “circulares” oscuros se deben a una acumulación subsuperficial de “carga” magnética la que no se observa en métodos más superficiales como el efecto Kerr magneto-óptico (d)

http://www.ifw-dresden.de/~schaefer/ToCBilder/2.2.htm

Efecto Kerr

<u>Efecto Kerr</u>: rotación de la dirección de polarización de un haz de luz polarizda al reflejarse en la superficie de un material magnético

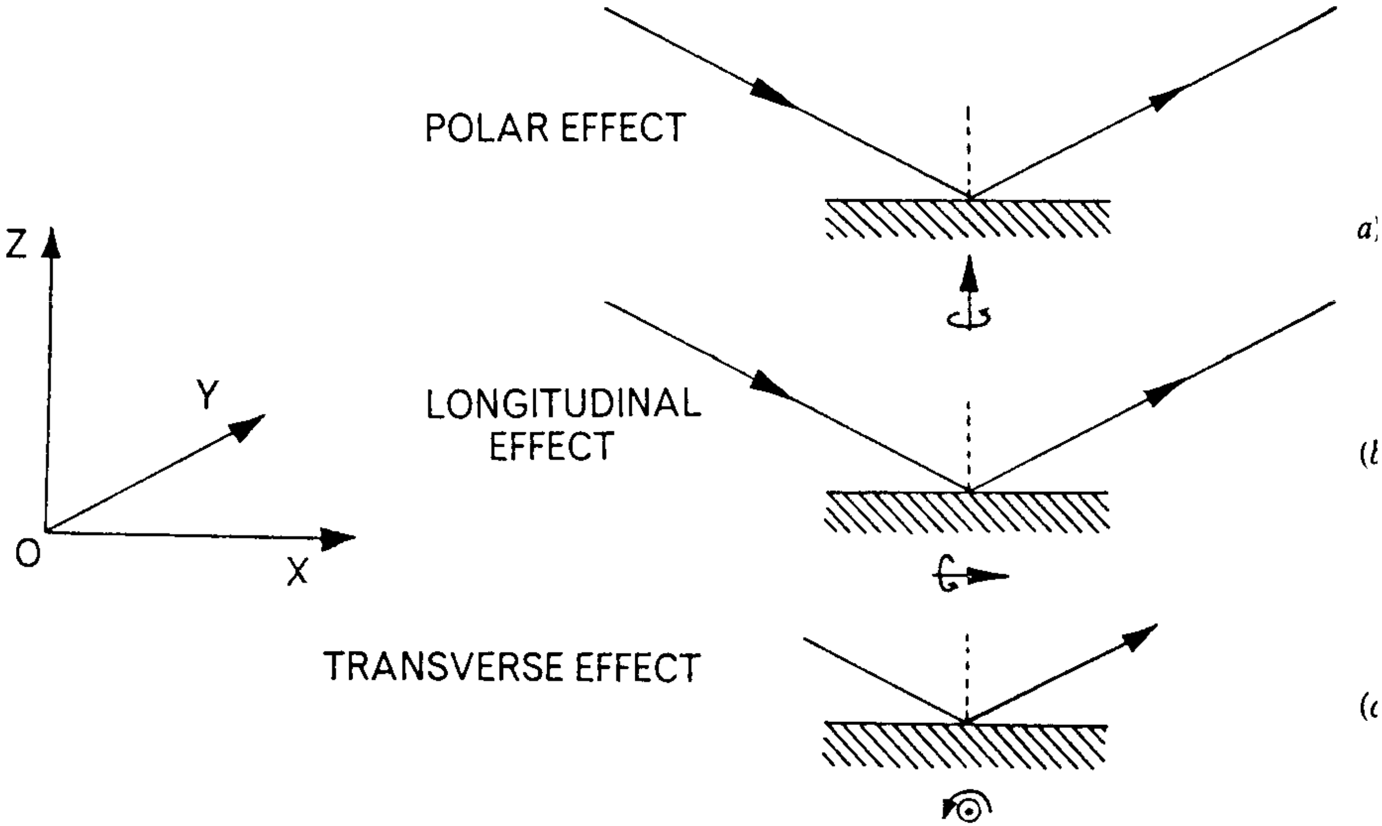

<u>polar</u>: rotación máxima de unos 20´
<u>longitudinal</u>: 4´
<u>transversal</u>: 4´

Efecto Kerr

El principio Kerr es que al reflejarse luz linealmente polarizada por un material magnetizado, rota el plano de polarización. Ello ocurre porque los índices de refracción de la luz polarizada circularmente a derecha y a izquierda son diferentes en presencia de magnetización. El ángulo de rotación producido por un material ferromagnético es generalmente de aprox. 1E-3 a 1E-2 grados, aunque se han observado ángulos mucho mayores en aleaciones de Tb-Fe-Co (un grado) y en compuestos de uranio (nueve grados). El ángulo de rotación es mayor cuando se incrementa el ángulo de incidencia. A partir del cambio de la intensidad Kerr (proporcional a la rotación Kerr y a la magnetización de la muestra) se construye la curva de histéresis en función del campo aplicado.

Microscopía de efecto Kerr

"Confocal" scanning Kerr microscope

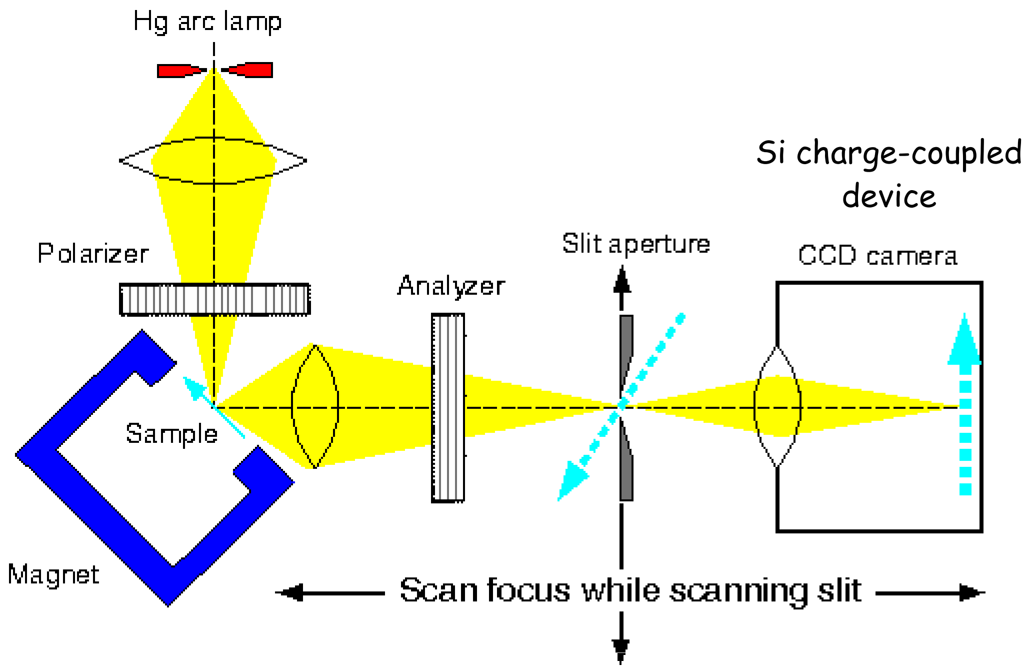

Images of 500 μm wide NiFe square

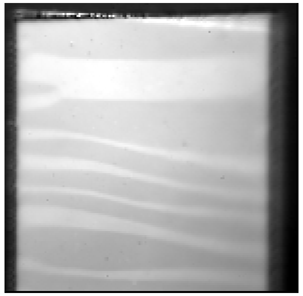

0 Oe field, no scanned slit

with confocal scanned slit

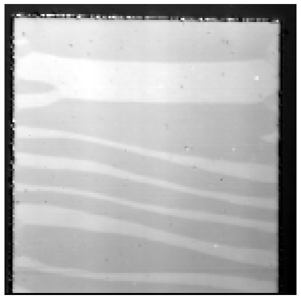

0 Oe field

−

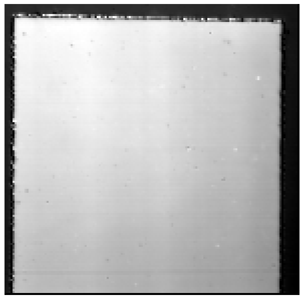

100 Oe field

=

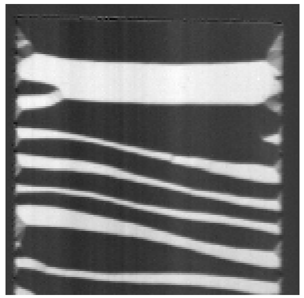

Difference

Efecto Kerr

Microscopía - imágenes

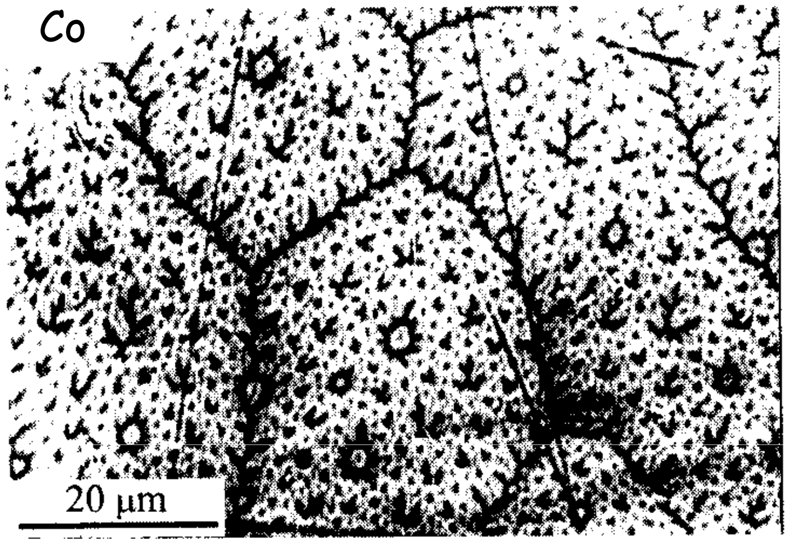

a)

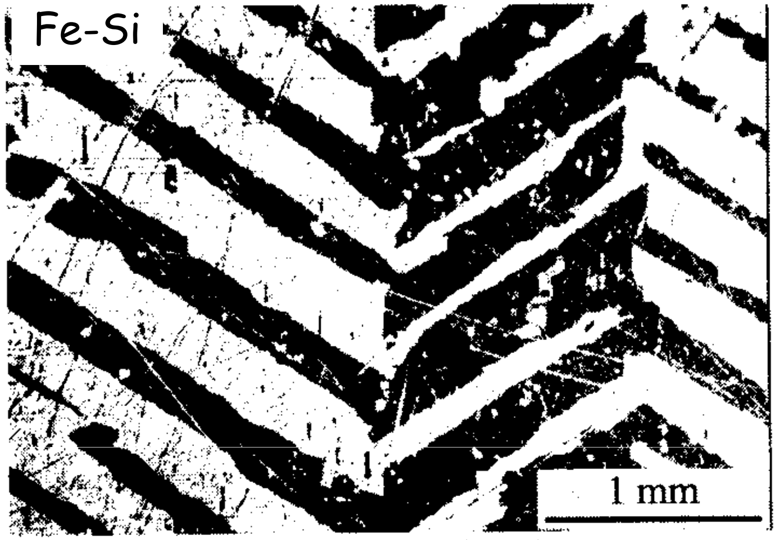

b) (110)

Fig. 2.9 Two examples of magneto-optical images from the time before the introduction of digital image processing. Branched domains on a cobalt crystal are shown in (a), taken by the polar Kerr effect in an applied field parallel to the easy axis. The overview picture (b) shows the "saw-tooth" pattern on a (110)-oriented silicon-iron crystal [124], taken with the longitudinal Kerr effect in a field perpendicular to the preferred axis of this material

Efecto Kerr

Imágenes de microscopía

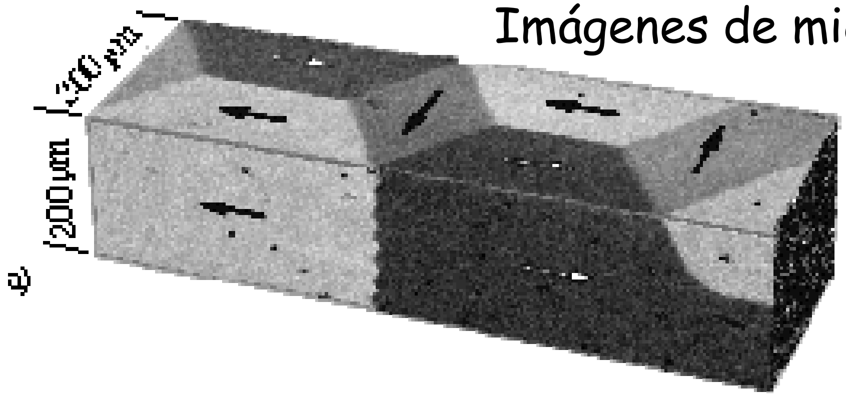

imagen Kerr
de dominios magnéticos,
observados en
dos lados de un trozo de Fe

http://www.ifw-dresden.de/~schaefer/ToCBilder/1.1.htm

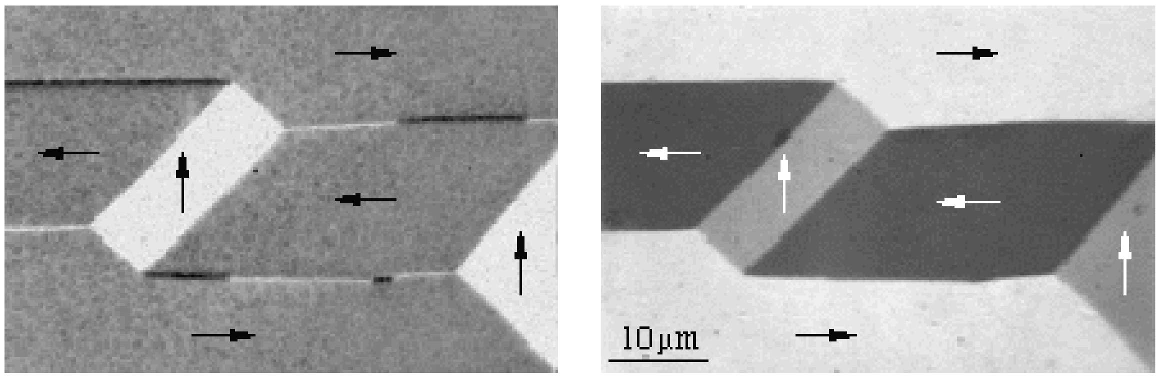

Dependiendo del plano de incidencia puede observarse el patrón de dominios (b) o la subestructura de las paredes de dominio (a). Sobre un cristal de SiFe orientado en la dirección (100)

mapas

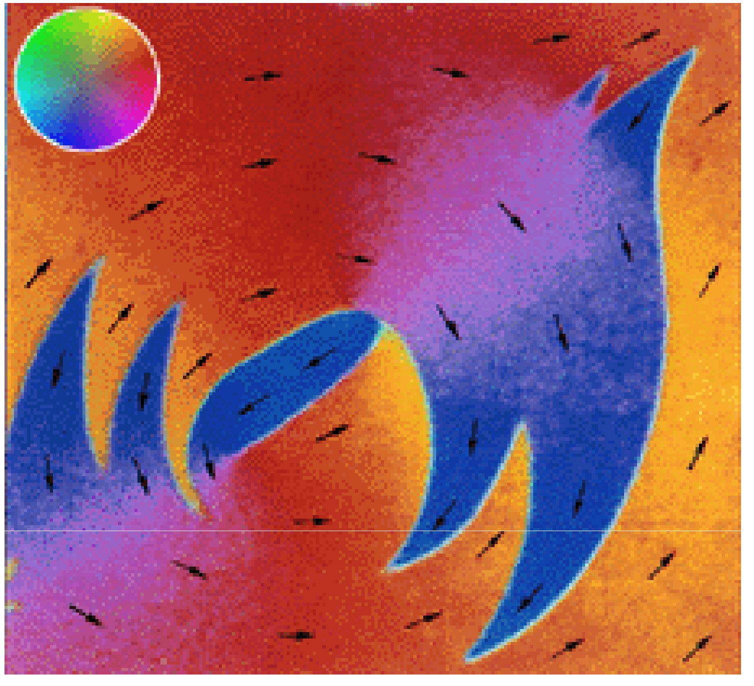

Microscopía Kerr cuantitativa. La magnetización superficial de un vidrio metálico se registra en un microscopio Kerr usando dos ejes con diferente sensibilidad. Se combina la información de ambas observaciones en una computadora y se representan en colores las direcciones de la magnetización

http://www.ifw-dresden.de/~schaefer/ToCBilder/Colour.htm

Magneto-optical Kerr effect (MOKE)

CU - Colorado Springs

Department of Physics and Energy Science

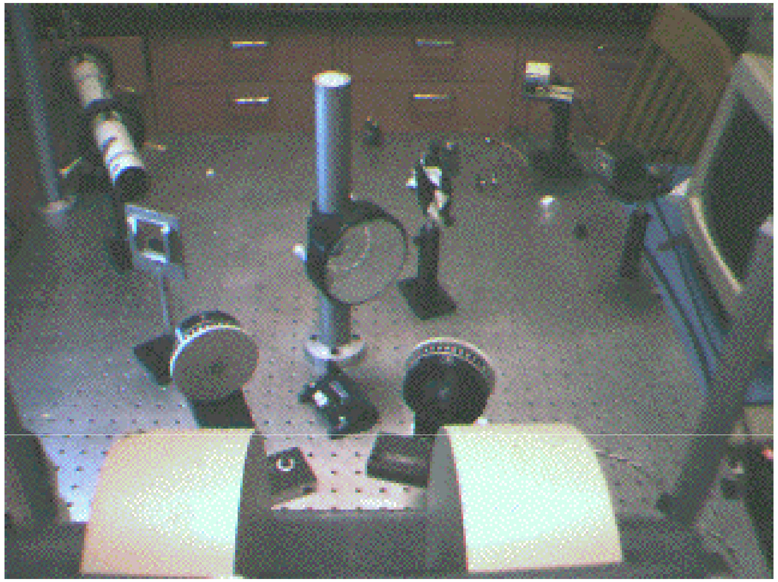

Este sistema usa un electroimán de 1Tesla. Utiliza un láser HeNe ultra-estable y polarizadores de alta calidad. El sistema de adquisición de datos produce las curvas de histéresis de películas delgadas magnéticas.

Magneto-optical Kerr effect at Washington University

Surface Magneto Optic Kerr Effect (SMOKE)

SMOKE: dispositivo para estudiar magnetismo superficial en películas ultradelgadas. Esta técnica fue iniciada por S.D. Bader y E.R. Moog a fines de los '80.

(Moog, E.R. and S.D. Bader. "Superlattices and Microstructures" Vol. 1:543 1985).

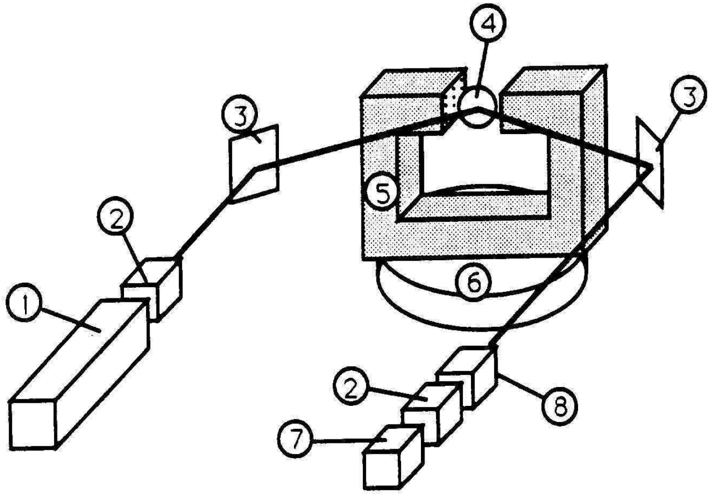

Note: (1) Laser, (2) polarizers, (3) mirrors, (4) sample, (5) magnetic core, (6) pulley, (7) photodetector, and (8) band-pass filter. This diagram is the measurement of longitudinal Kerr Effect and the external field is in the plane of sample. The electromagnet can be rotated by means of the pulley through a push-pull rod.

O Magnetômetro a Efeito Kerr e o filme fino de Co/Si

Hugo Bonette de Carvalho
Universidade Estadual de Campinas
Instituto de Física Gleb Wathagin

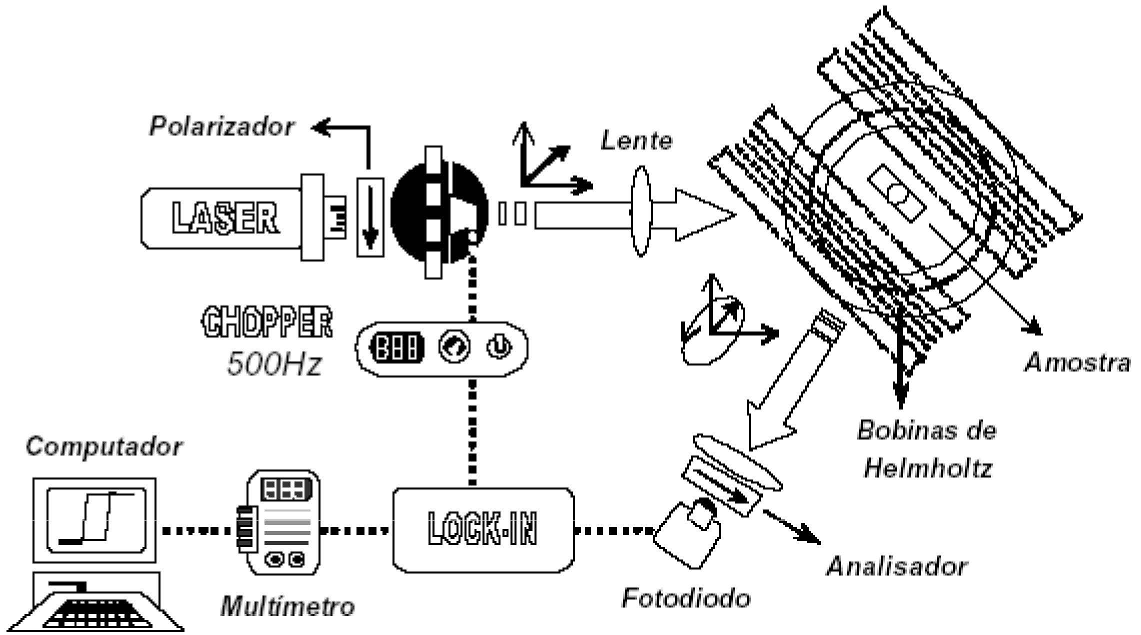

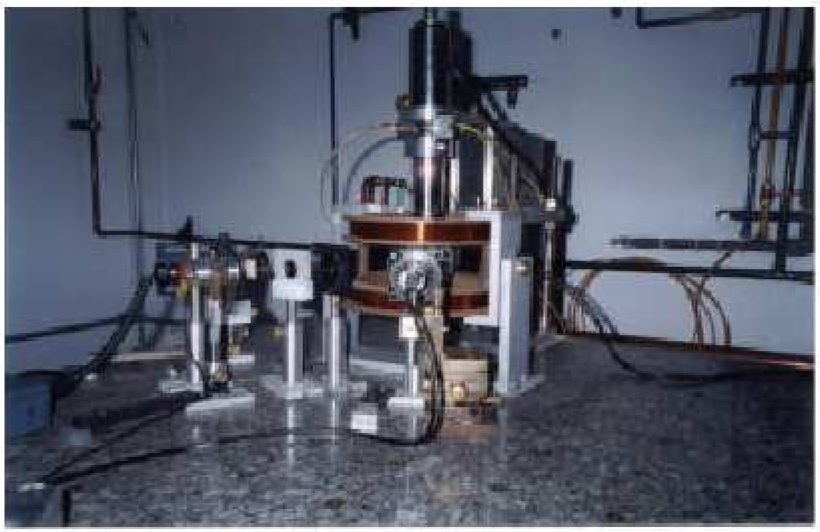

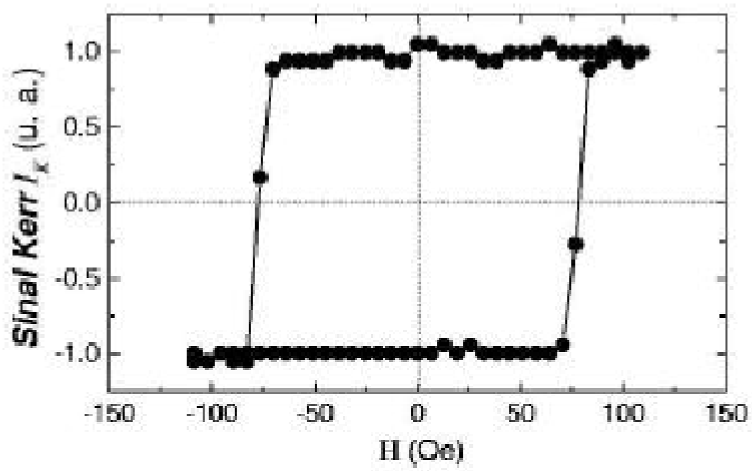

Fig. 3.8 - Histerese obtida para o filme de Co/Si de 160Å no modo Transversal.

Magneto-optical storage technology

As implied by the name, these drives use a hybrid of magnetic and optical technologies, employing laser to read data on the disk, while additionally needing magnetic field to write data. An MO disk drive is so designed that an inserted disk will be exposed to a magnet on the label side and to the light (laser beam) on the opposite side. The disks, which come in 3.5in and 5.25in formats, have a special alloy layer that has the property of reflecting laser light at slightly different angles depending on which way it's magnetised, and data can be stored on it as north and south magnetic spots, just like on a hard disk.

While a hard disk can be magnetised at any temperature, the magnetic coating used on MO media is designed to be extremely stable at room temperature, making the data unchangeable unless the disc is heated to above a temperature level called the Curie point, usually around **200** degrees centigrade. Instead of heating the whole disc, MO drives use a laser to target and heat specific regions of magnetic particles. This accurate technique enables MO media to pack in a lot more information than other magnetic devices. Once heated the magnetic particles can easily have their direction changed by a magnetic field generated by the read/write head.

Lectura

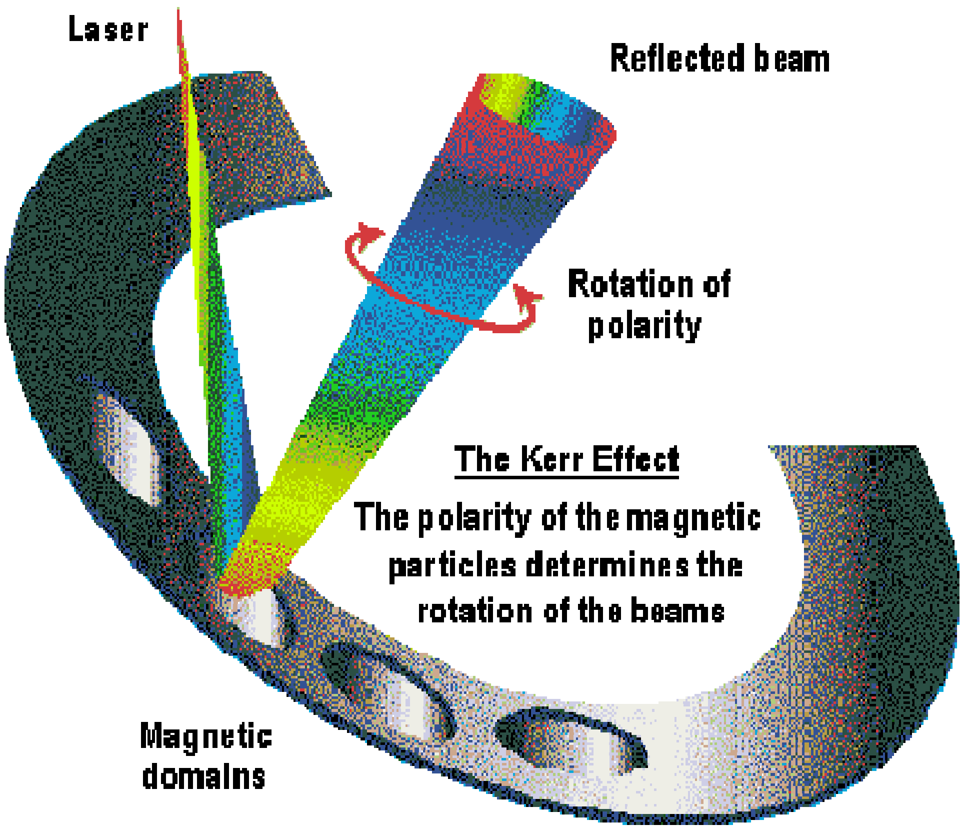
Laser
Reflected beam
Rotation of polarity
The Kerr Effect
The polarity of the magnetic particles determines the rotation of the beams
Magnetic domains

Information is read using a less powerful laser, making use of the Kerr Effect, where the polarity of the reflected light is altered depending on the orientation of the magnetic particles. Where the laser/magnetic head hasn't touched the disk, the spot represents a "0", and the spots where the disk has been heated up and magnetically written will be seen as data "1s".

However, this is a "two-pass" process which, coupled with the tendency for MO heads to be heavy, resulted in early implementations being relatively slow. Nevertheless, MO disks can offer very high capacity and fairly cheap media as well as top archival properties, often being rated with an **average life of 30 years** - far longer than any magnetic media.

Magneto-optical technology received a massive boost in the spring of 1997 with the launch of Plasmon's DW260 drive which used LIMDOW technology to achieve a much increased level of performance over previous MO drives.

Efecto Faraday

Efecto Faraday: Como el Kerr, pero por transmisión. Para láminas delgadas de óxidos ferromagnéticos o películas metálicas.

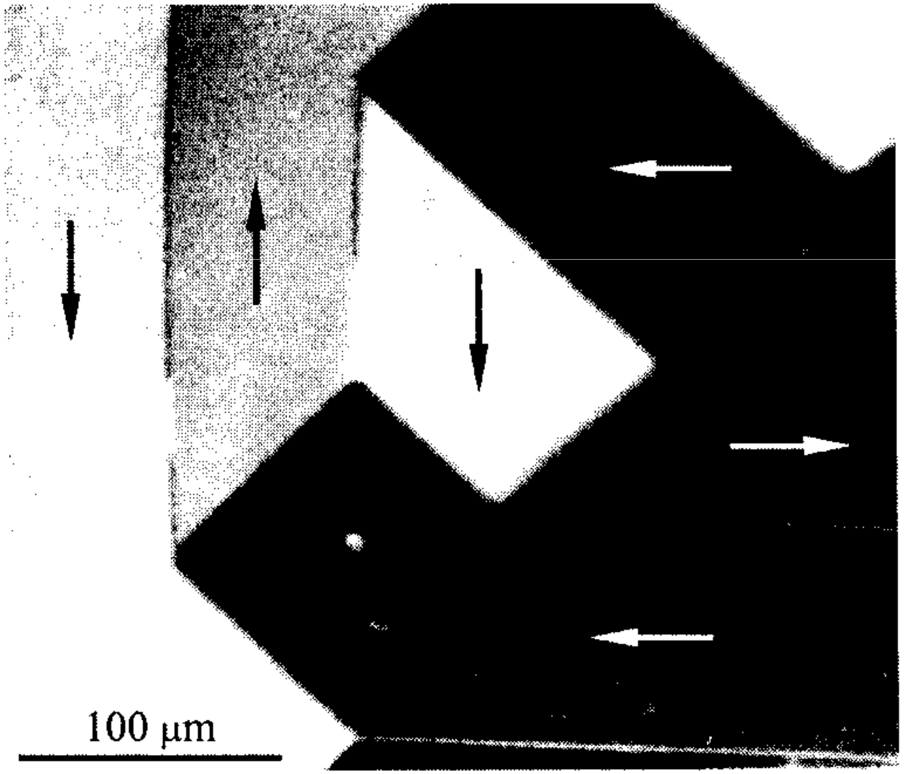

Fig. 2.21 A transmission image of a modified YIG garnet plate. Because of a small cobalt content, the easy axes in this garnet are ⟨100⟩. We see mainly the Voigt effect in the domains differing by 90°, and the polar Faraday effect in the 180° domain walls. The illumination is almost perpendicular, but a slight tilting (along the vertical axis in the picture) generates some longitudinal Faraday contrast between the 180° domains, too. (Together with *M. Rührig*, Erlangen. Sample: courtesy *W. Tolksdorf*, Philips Hamburg)

Microscopía Lorentz-TEM

Microscopía Lorentz-TEM: Para espesores de hasta unos 200 nm. Los electrones transmitidos son deflectados por la fuerza de Lorentz **F** = -e**v**xB. El ángulo de deflexión es pequeño (típicamente 0.01° en Fe). Es necesario sobre o sub enfocar la imagen porque al modificar el foco las imágenes de dominios con magnetizaciones diferentes se mueven en direcciones diferentes. Se pueden obtener resoluciones de hasta 5 nm. La muestra debe apantallarse magnéticamente.

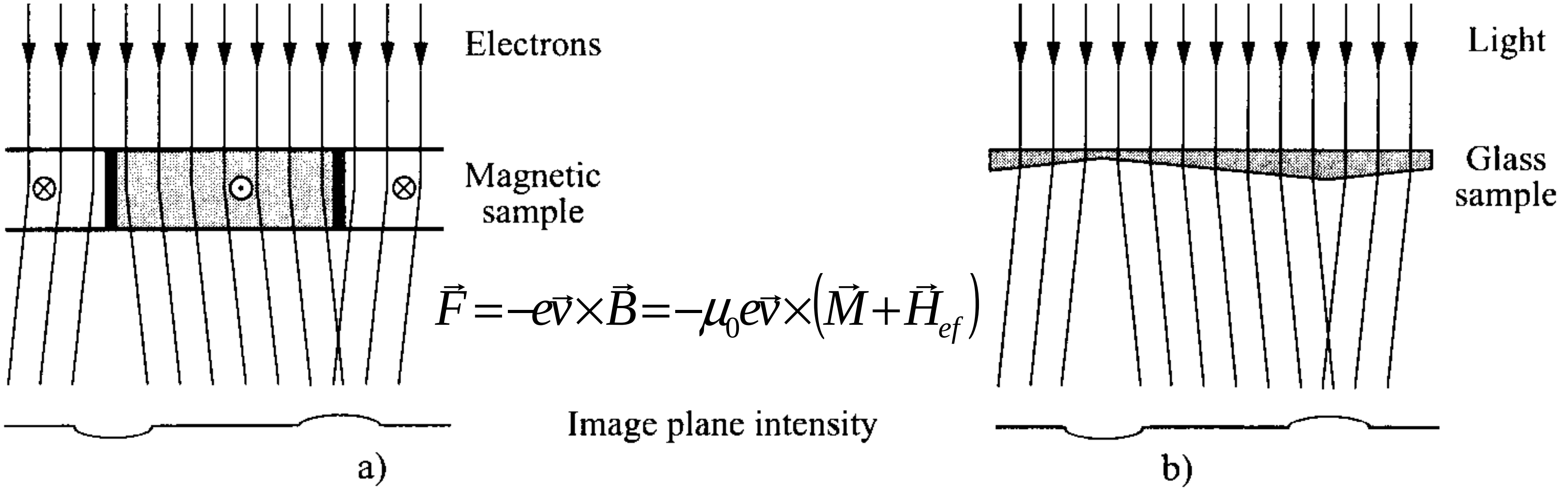

$$\vec{F} = -e\vec{v}\times\vec{B} = -\mu_0 e\vec{v}\times\left(\vec{M}+\vec{H}_{ef}\right)$$

Fig. 2.25 Electron deflection in the shadow, or "Fresnel" mode (a). The microscope is focused some millimetres below the sample. (b) Optical analogue of (a)

Transmission electron microscopy

Schematic of magnetic contrast generation in the Fresnel and Foucault modes of Lorentz TEM. The Fresnel intensity indicates that only domain walls are delineated, whilst the Foucault intensity is constant within the interior of the domain and only changes at domain walls.

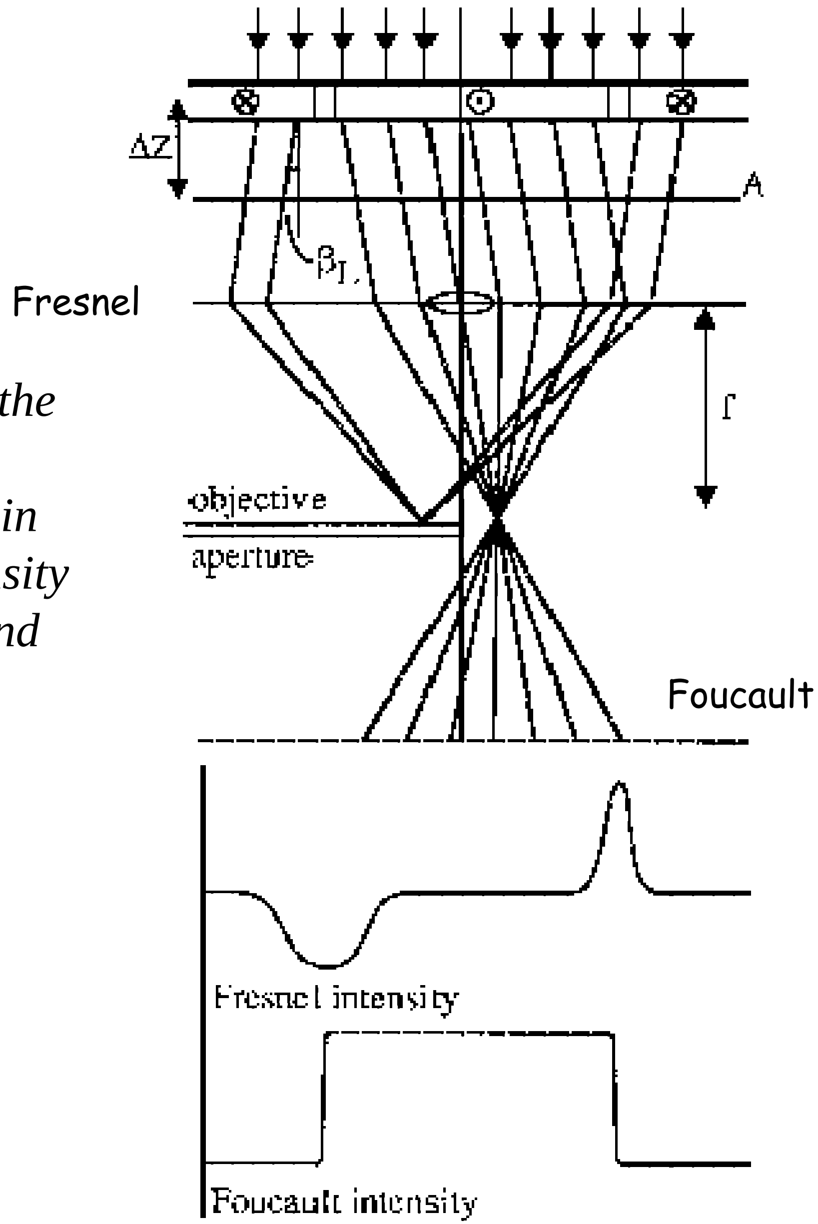

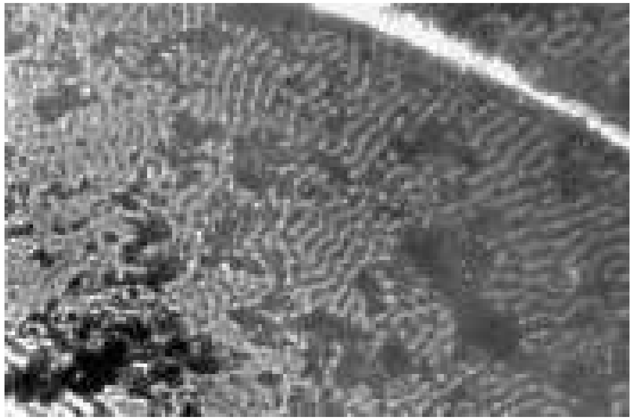

Fresnel *image of magnetic domains in a* ***CoNi/Pt multilayer.***
This maze type domain structure is typical for films with perpendicular anisotropy.

Fresnel *image of magnetic domains and ripple contrast in a magnetically soft* ***Co/Cu multilayer*** *which exhibits GMR.*
The ripple is always orthogonal to the direction of magnetisation within a domain.

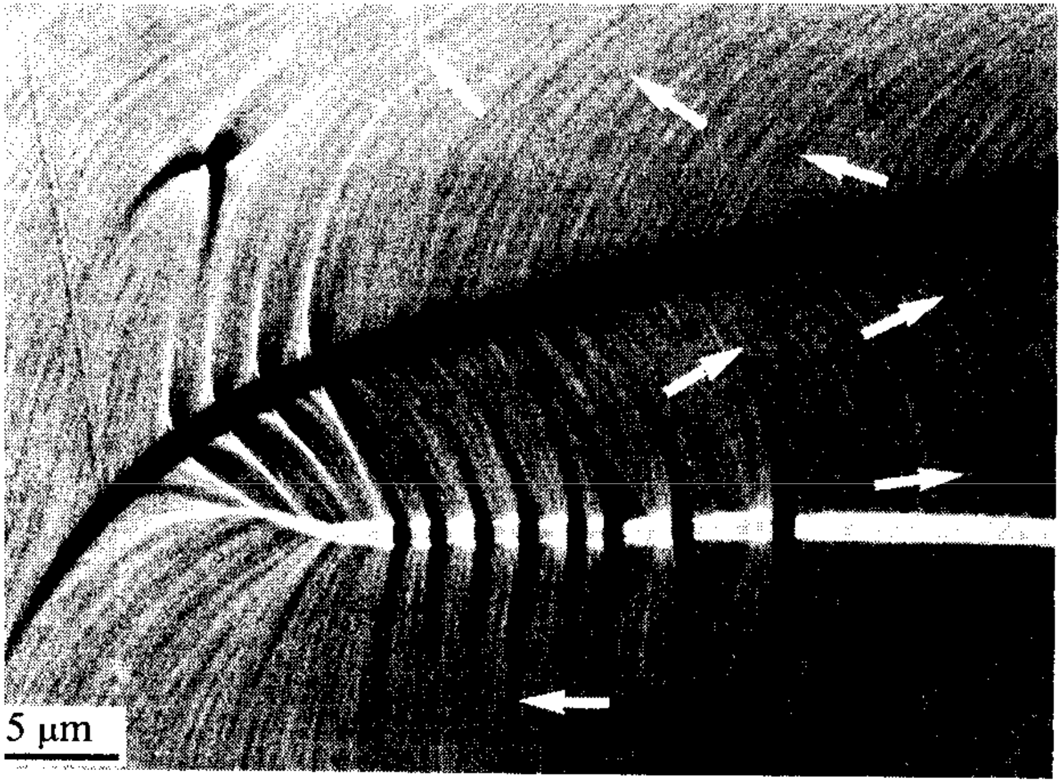

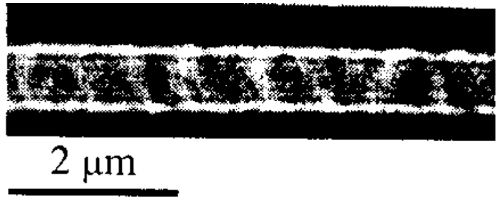

Fig. 2.26 Lorentz picture of a polycrystalline Permalloy film showing the streaky *ripple* texture perpendicular to the mean magnetization in the domains and *cross-tie* walls. The convergent wall displays diffraction fringes as shown in the enlargement. (Courtesy *S. Tsukahara* [261])

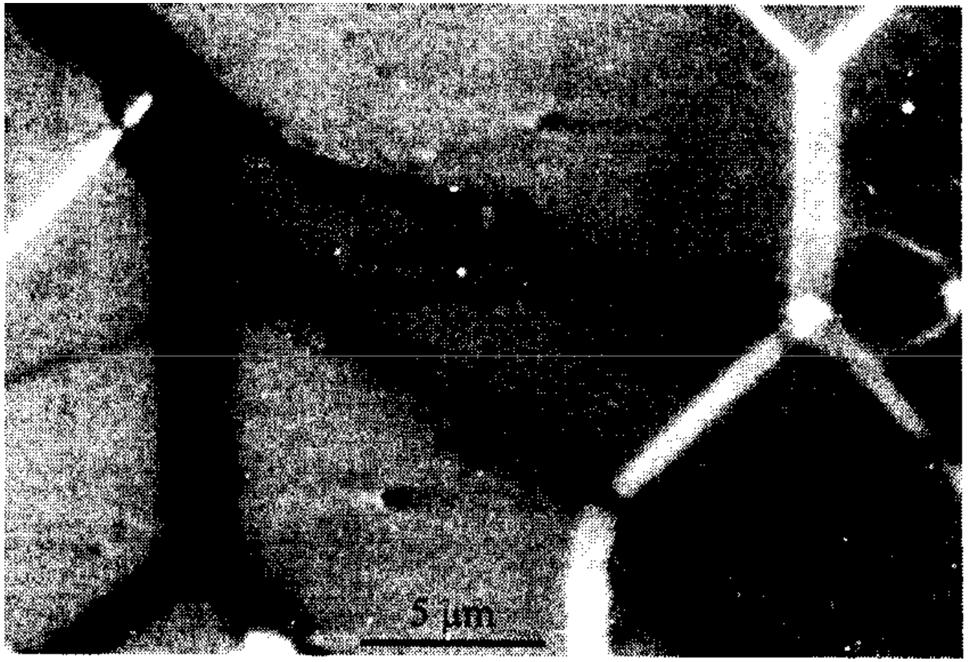

Fig. 2.27 A defocused mode Lorentz picture from a (100)-oriented single-crystal iron sample of unknown thickness. Note the asymmetric profile of the divergent (black) wall which reflects the internal structure of the asymmetric Bloch wall (Sect. 3.6.4D). The irregular lines are lattice contrasts. (Courtesy *S. Tsukahara* [261])

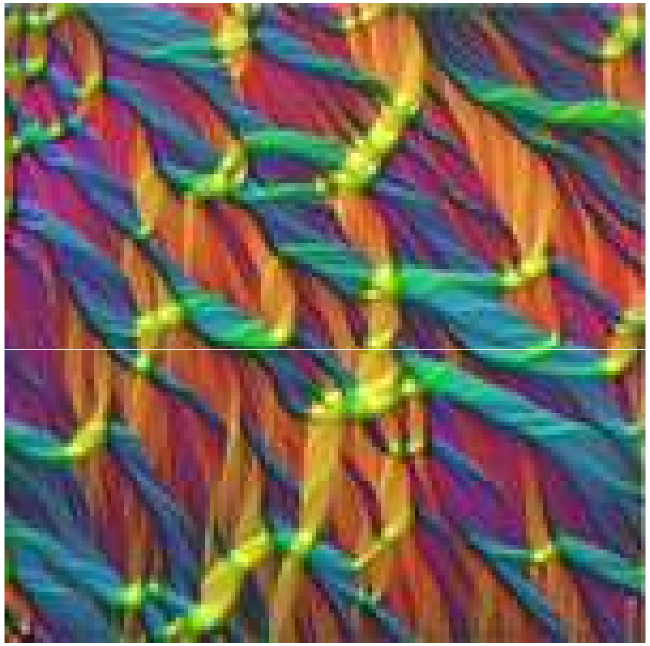

Magnetic domains in a thin cobalt film

The colours in the image show the different directions of the magnetic field in a layer of polycrystalline cobalt that has a thickness of only 20nm. The direction of the magnetic field in the film changes at the positions of domain walls. The field of view is approximately 200µm. The image was acquired using the **Fresnel** mode of Lorentz microscopy in a field emission gun transmission electron microscope. It was recorded out of focus to enhance the contrast of the domain walls, and then converted to a colour induction map by applying the Transport of Intensity Equation to the image intensity

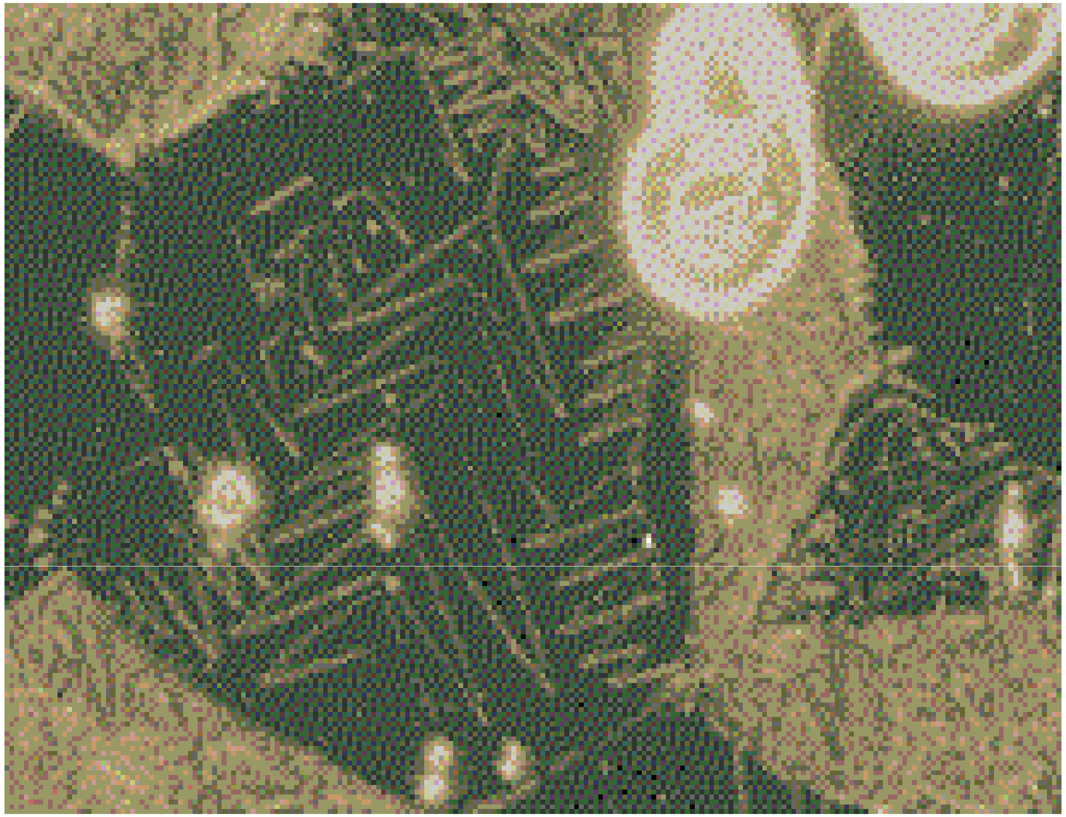

The image is changing domain patterns of silicon steel according to successively changing magnetic field of +2.4, 0 and -2.4 kA/m.
It is dark-field microscopic image of Colloid A-07-dropped specimen.
Changes of triangular shapes and sizes of domains are clearly seen.

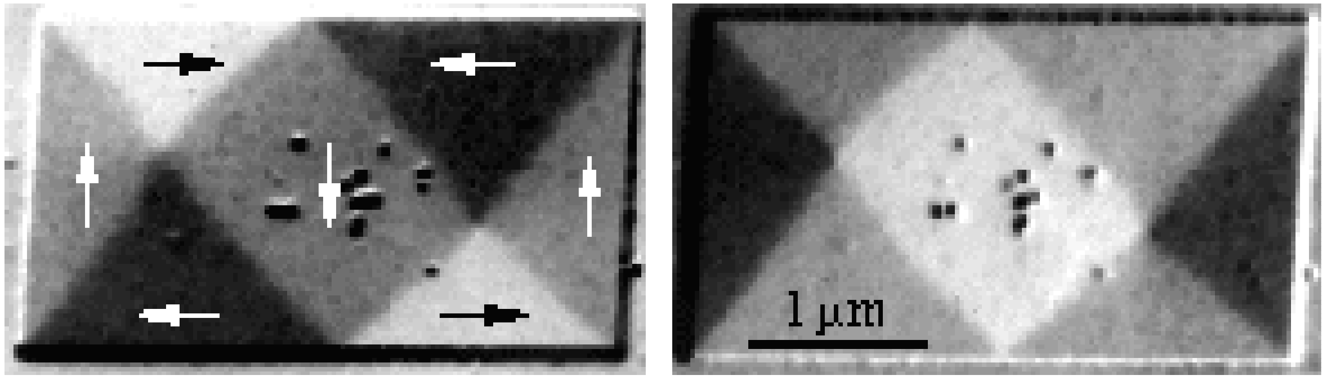

Fig. 2.30 The Differential Phase Contrast method of transmission electron microscopy offers quantitative information at high resolution. The pictures show the horizontal (a) and the vertical (b) magnetization components of a closed-flux domain pattern in a thin-film Permalloy element

(*J.N. Chapman*)

http://www.ifw-dresden.de/~schaefer/ToCBilder/2.4.htm

Electron Reflection and Scattering Methods

<u>SEM</u>: basada también en el efecto de la fuerza de Lorentz

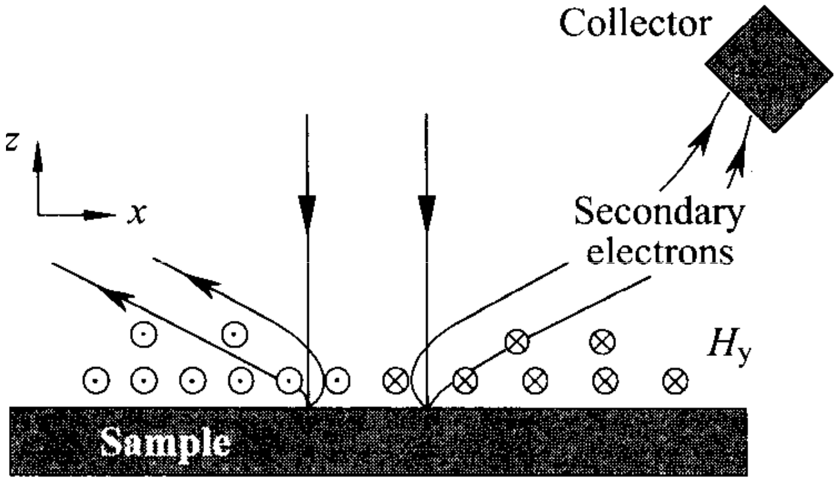

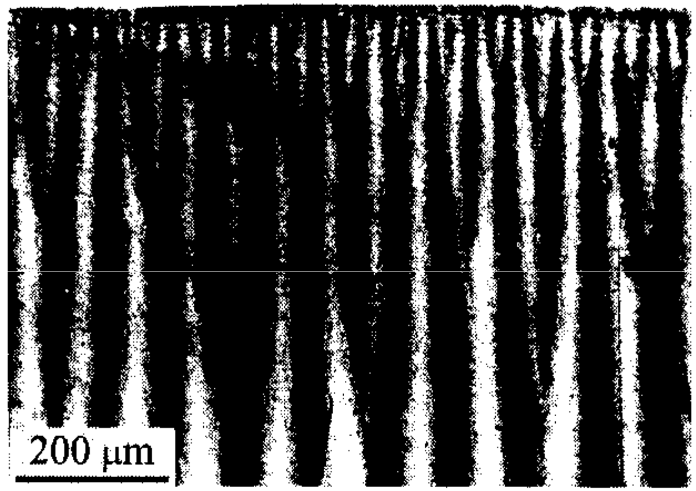

Fig. 2.33 Schematic of Type I contrast (a). The secondary electrons of the two beams see different fields and are deflected into different directions. (b) Domains on a cobalt crystal (edge view) as a typical example for this technique. (Courtesy *J. Jakubovics* [312])

Electron Reflection and Scattering Methods

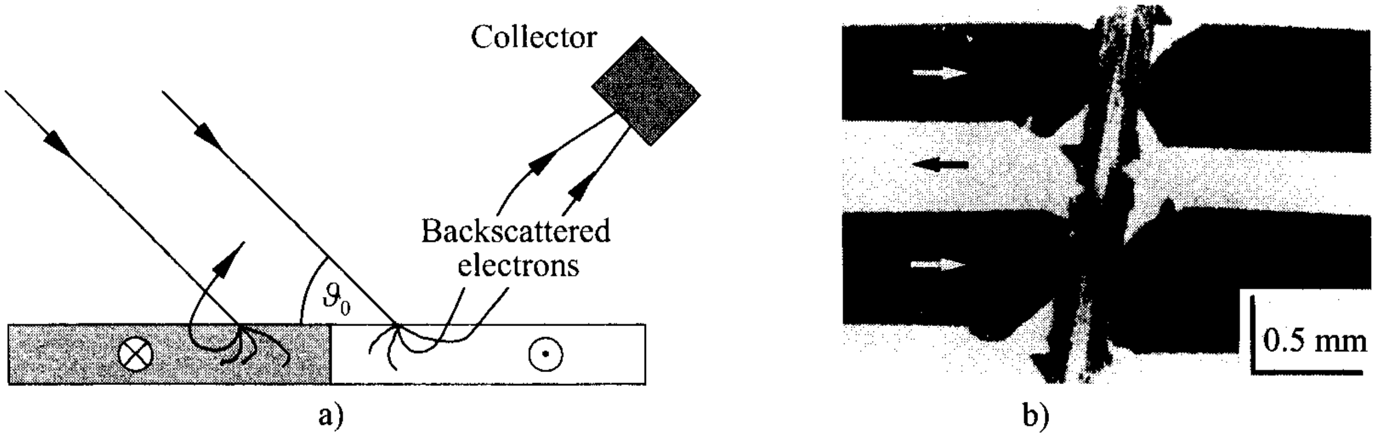

Fig. 2.34 Backscattering contrast in the SEM (a) with some typical electron paths inside the sample, and an image of a silicon-iron transformer steel sample (b) showing domains near a scratch introduced for the purpose of domain refinement. (Courtesy *T. Nozawa* [332])

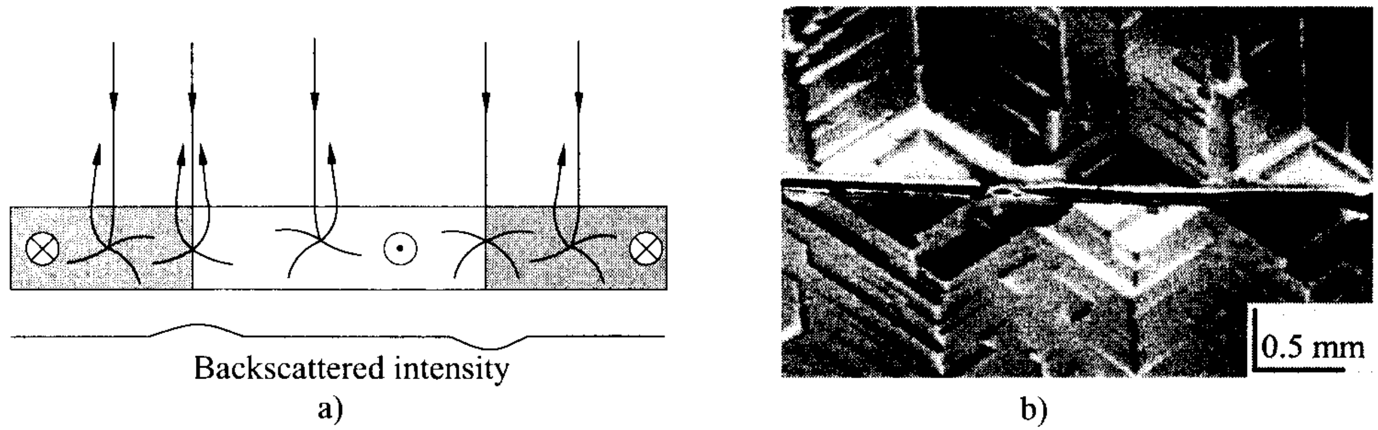

Fig. 2.35 Domain boundary contrast formation in the SEM at oblique incidence with the plane of incidence parallel to the domain walls (a). The backscattering probability is larger near the left than near the right wall. (b) Boundary contrast on a (100) SiFe crystal, together with domain contrast from closure domains near a scratch. (Courtesy *J.P. Jakubovics*)

Magnetic Force Microscopy

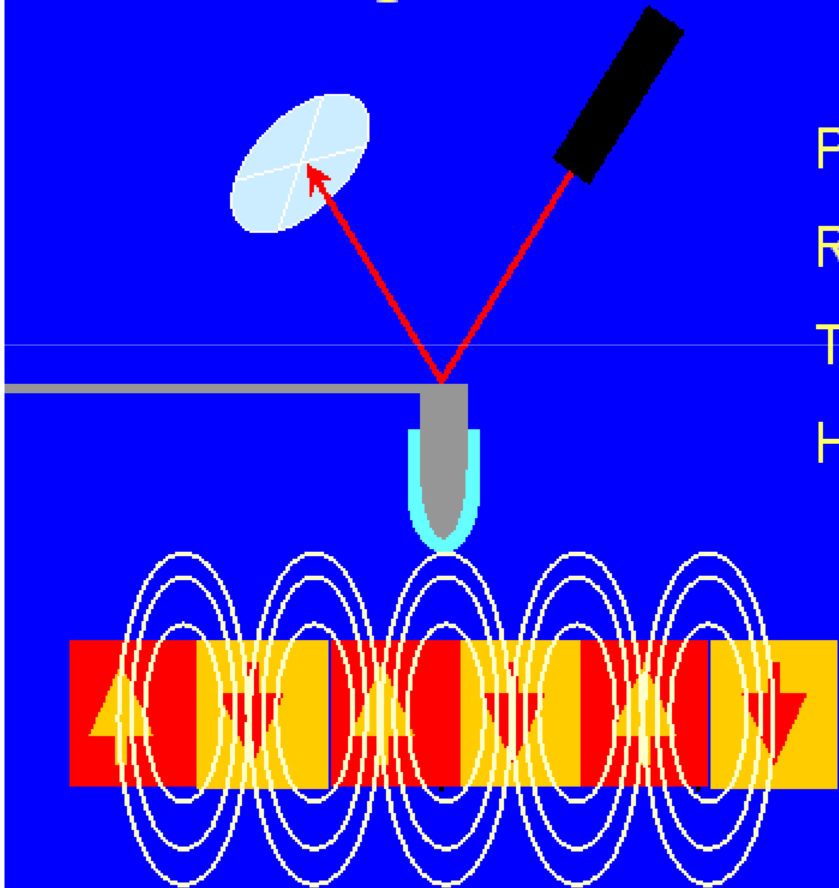

Probes stray fields

Resolution ~40 nm

Tip-sample interactions

High fields / low temperatures difficult

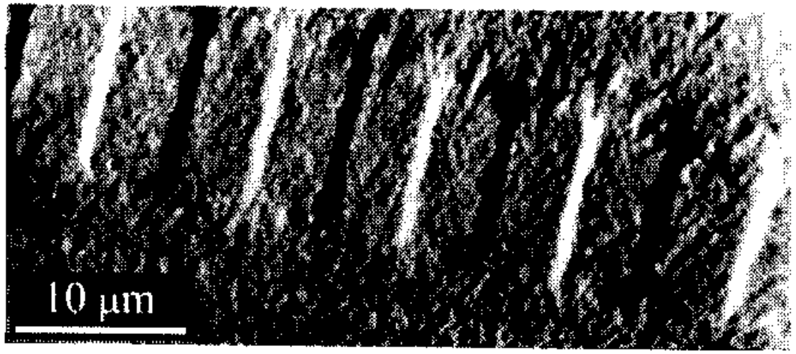

Fig. 2.40 Written longitudinal recording track pattern observed in a magnetic force microscope, displaying the magnetic charges at the transitions. (Courtesy *D. Rugar*, IBM Research)

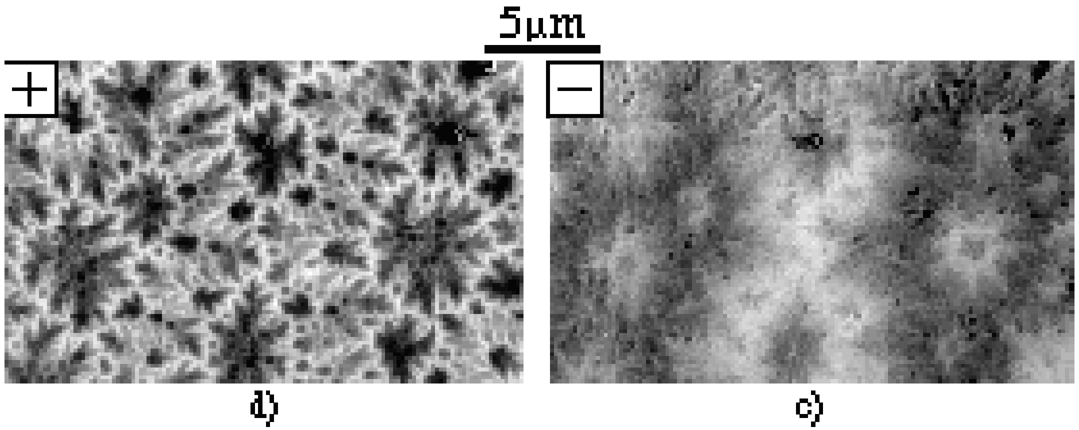

Fig. 2.43d,e **Magnetic force microscopy** on the basal plane of a cobalt crystal. Image processing can reveal "susceptibility contrast" (d) and "charge contrast" (e), two imaging modes which are unavailable with other techniques. (d) and (e) are the sum and the difference of images taken with opposite polarity of the tip magnetization, respectively

http://www.ifw-dresden.de/~schaefer/ToCBilder/2.6.htm

Magnetic Materials

Finished magnetic heads can be measured for their performance and response to signal and noise fields. Devices can also be examined using the Bitter Pattern System to locate magnetic domain irregularities.

Magnetic Recording Imaging

Magnetic force microscopy images of recorded media (tape, disk, film) made with our scanning probe microscope can provide insight into problems that may exist within a recording system, such as tracking error, head to media spacing, and media jitter.

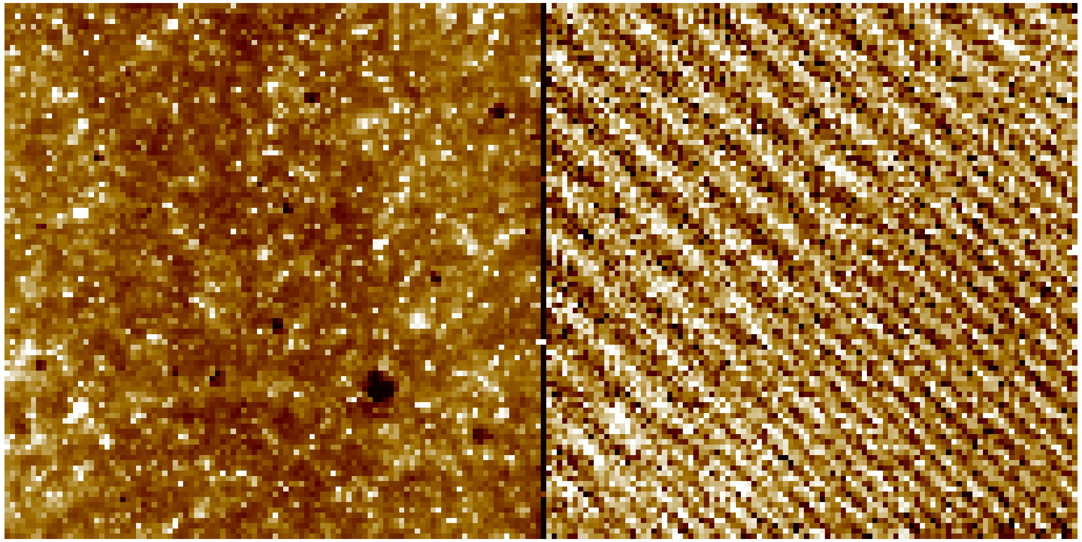

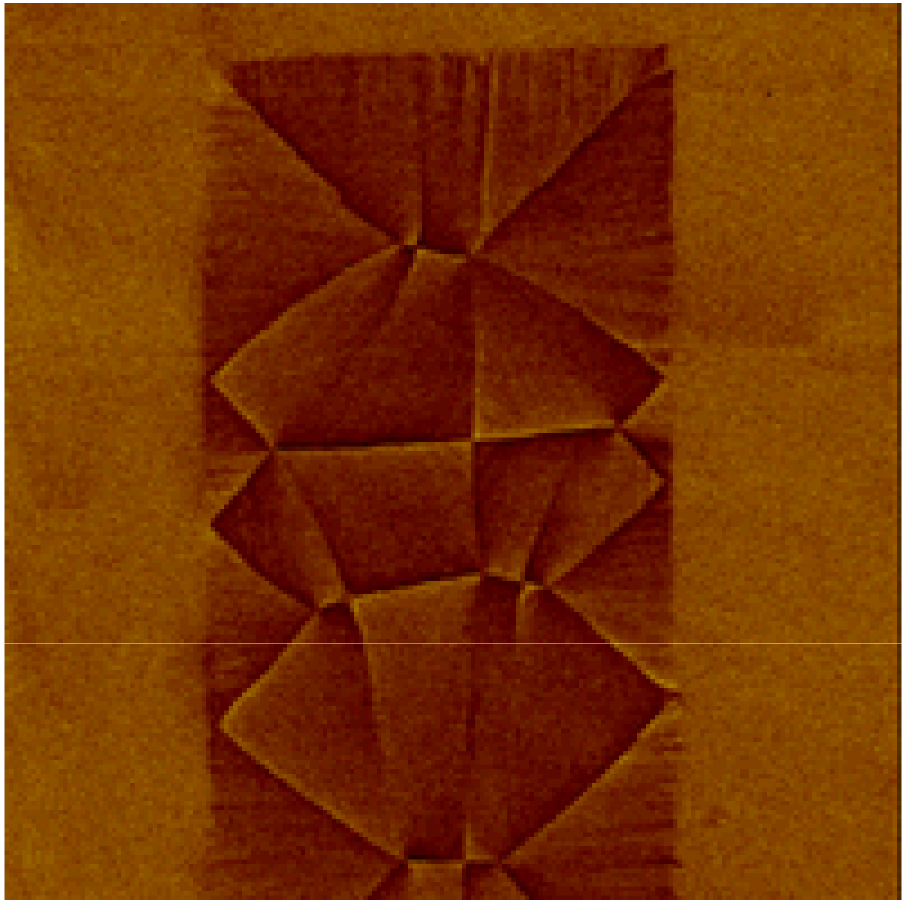

Magnetic domains in low-coercivity, amorphous CoZrNb film used in emerging, high-M_s thin-film heads. 50µm scan. Visible are Landau-Lifshitz and cross-tie domains, and the effects of edge roughness. Such images surpass the resolution of optical Kerr-effect. Captured with LiftMode (lift height 75nm) and a low-moment tip to prevent domain perturbation.

Magnetic stripe-domains in a-$GdFe_2$ films

MFM

thickness:

33 nm | 65 nm | 1000 nm

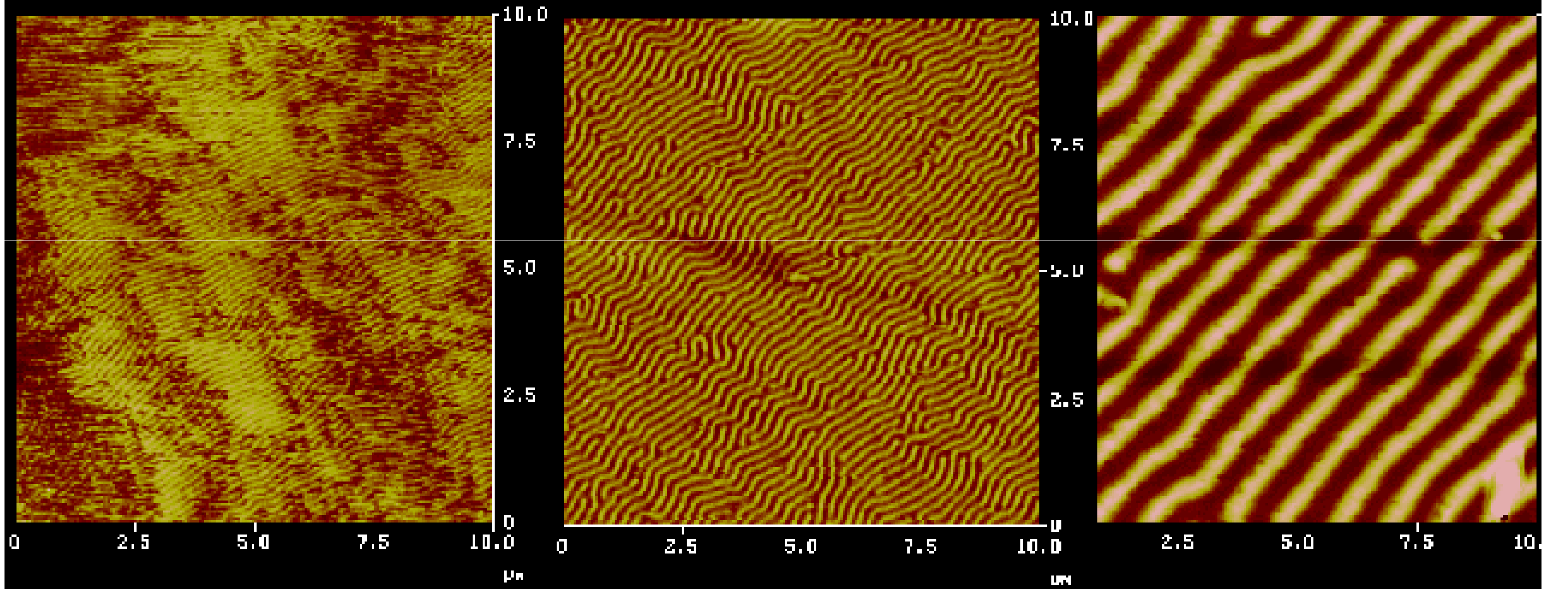

period: 150 nm | 210 nm | 830 nm

area: $10\times10\ \mu m^2$

Reorientation transition of ultrathin cobalt films on Au(111)

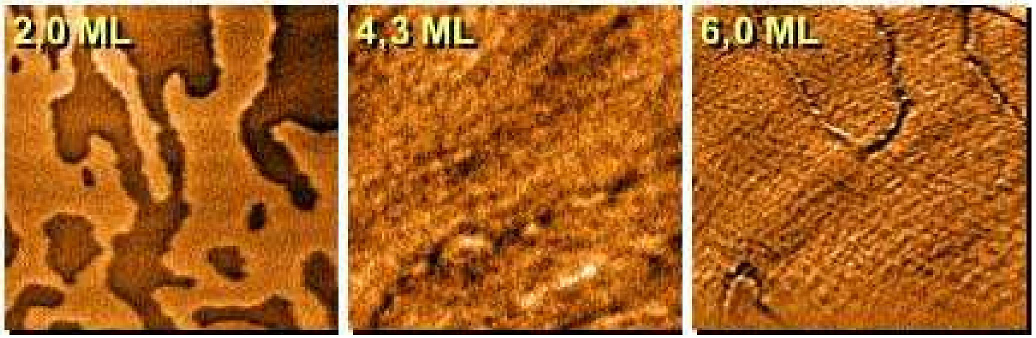

Three **MFM** images of cobalt deposited on gold. The numbers within the images indicate the nominal film thickness in monolayers. Tip magnetization is perpendicular to the surface. At low coverages (2 ML) bright and dark areas, which correspond to out-of-plane domains are observed. The contrast vanishes at 4.3 ML coverage. At 6 ML coverage the magnetic contrast reappears, but now domain walls are imaged - a typical signature of domains with in plane magnetization. The observed contrast change clearly indicates a thickness dependent reorientation of the magnetization direction in the cobalt film.

Domain Growth on $La_{0,7}Ca_{0,3}MnO_3$

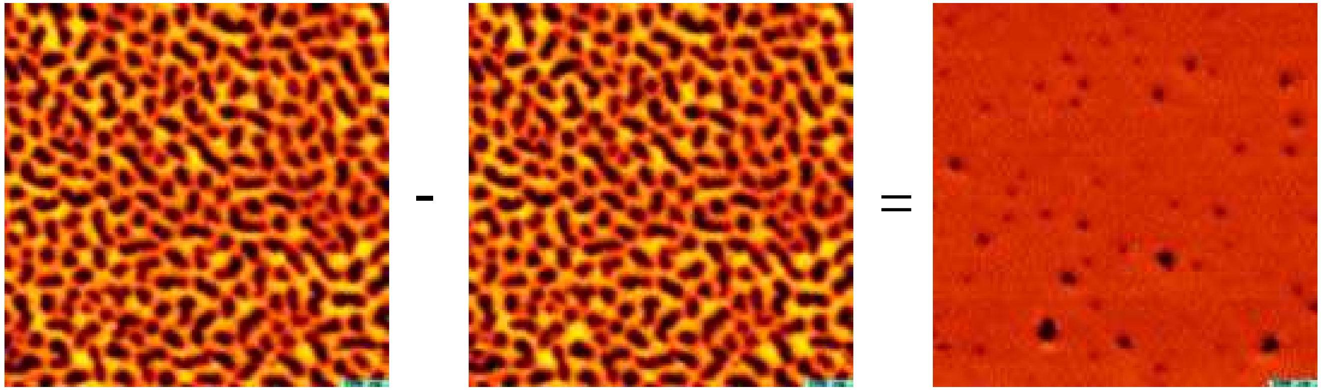

H H+ΔH

The stability at low temperatures and the careful microscope design enable a detailed study of domain growth in external magnetic fields. The two images on the left show the maze type domain structure of an perovskite manganite thin film in two slightly different external magnetic fields. Bright areas indicate regions, where tip and sample magnetization is parallel (attractive magnetostatic interaction), while dark areas indicate an antiparallel configuration (repulsive magnetostatic interaction). It is difficult to detect any difference. However, after subtracting one image from the other, those areas, which changed their magnetization direction become clearly visible as dark spots in the right image.

Investigation of magnetic bit structures

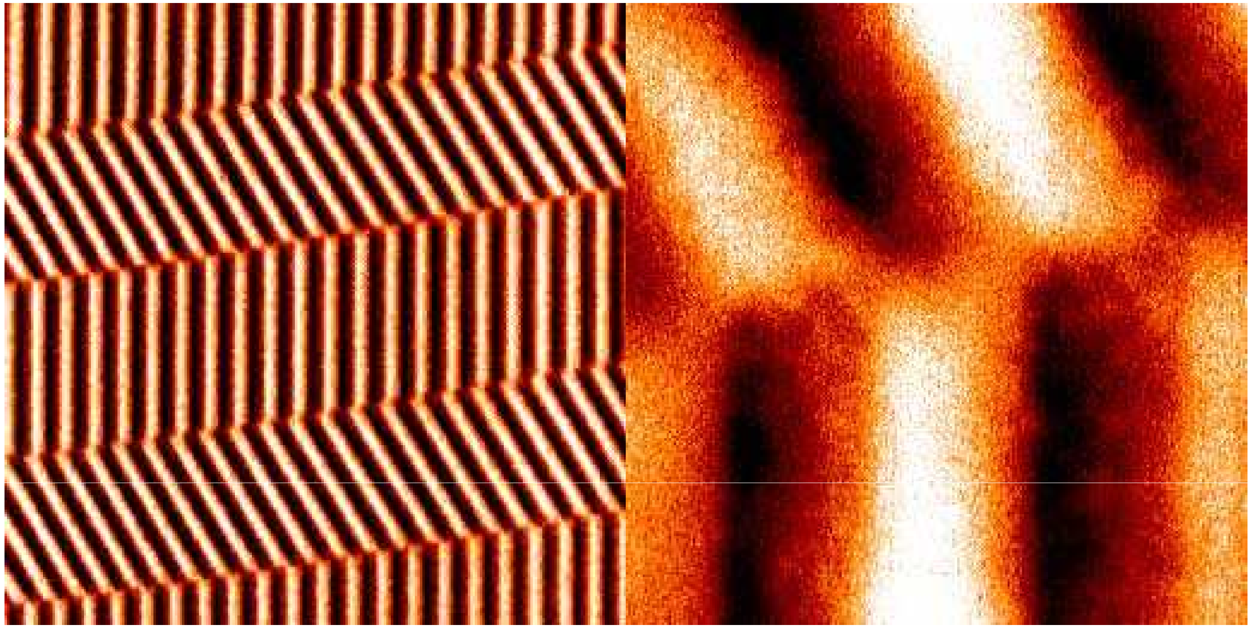

Two MFM images of closely spaced bit tracks on a tape, which is used as mass data storage device. While the read head can only disinguish "1" and "0" along the tracks, MFM is able resolve the fine structure of the magnetic bit structure. Regarding device optimations the area where neighbouring meet (right image) are of particular importance to increase the bit density.

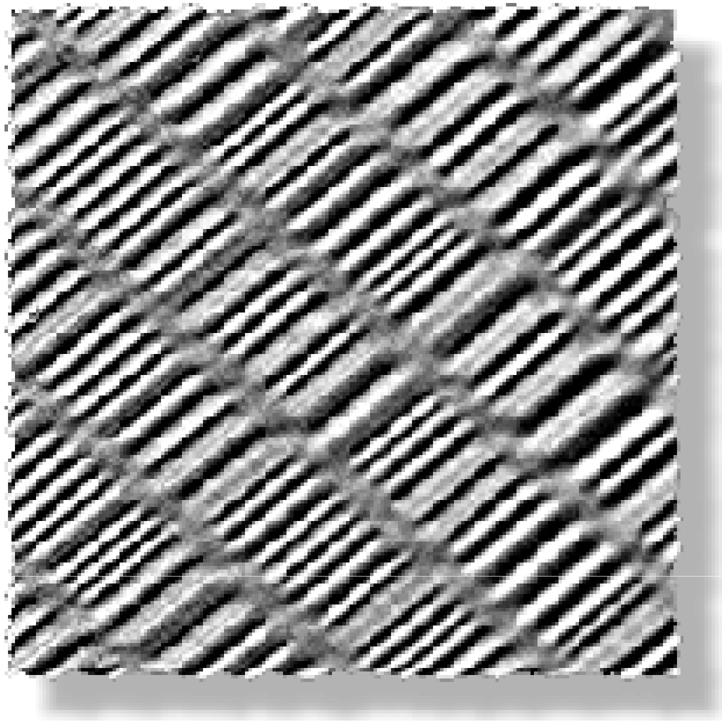

MFM image showing the bits of a hard disk. Field of view 30µm

Topology and dynamics of magnetic domains

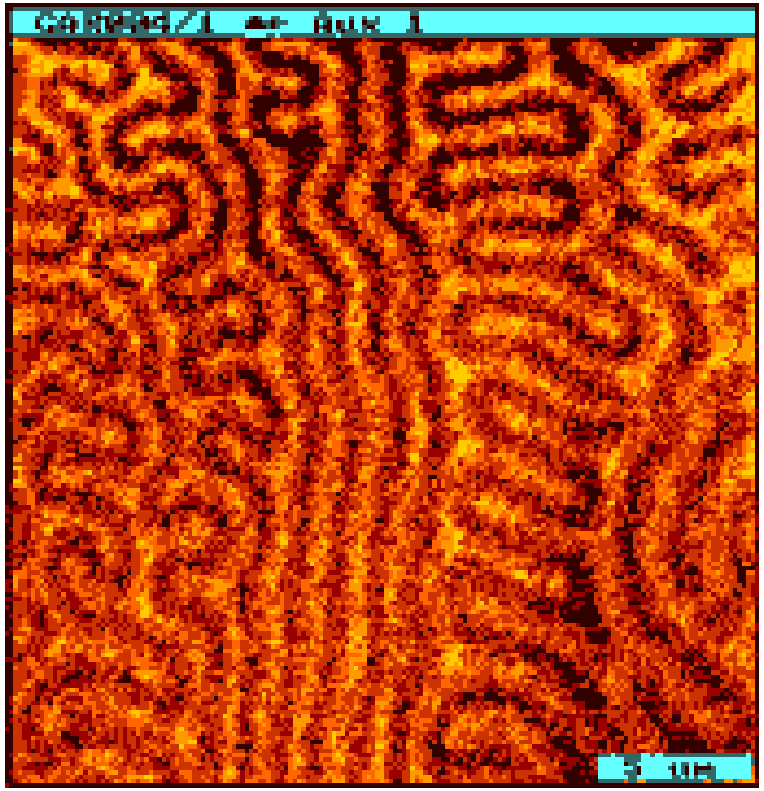

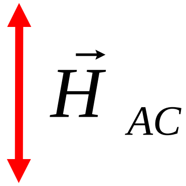

In soft magnetic materials with perpendicular anisotropy such as yttrium iron garnets, domains form a labyrinthine structure in the demagnetized state. This structure is also observed in other physical systems, such as ferrofluids, Langmur films, oscillatory chemical reactions, polymers and many other. It appears, that the local mobility of the domain walls is closely related to the domain topology. We do imaging studies of the domain wall responce to a periodic and non-periodic magnetic drive and investigate depinning and creep phenomena in labyrinthine domain structures.

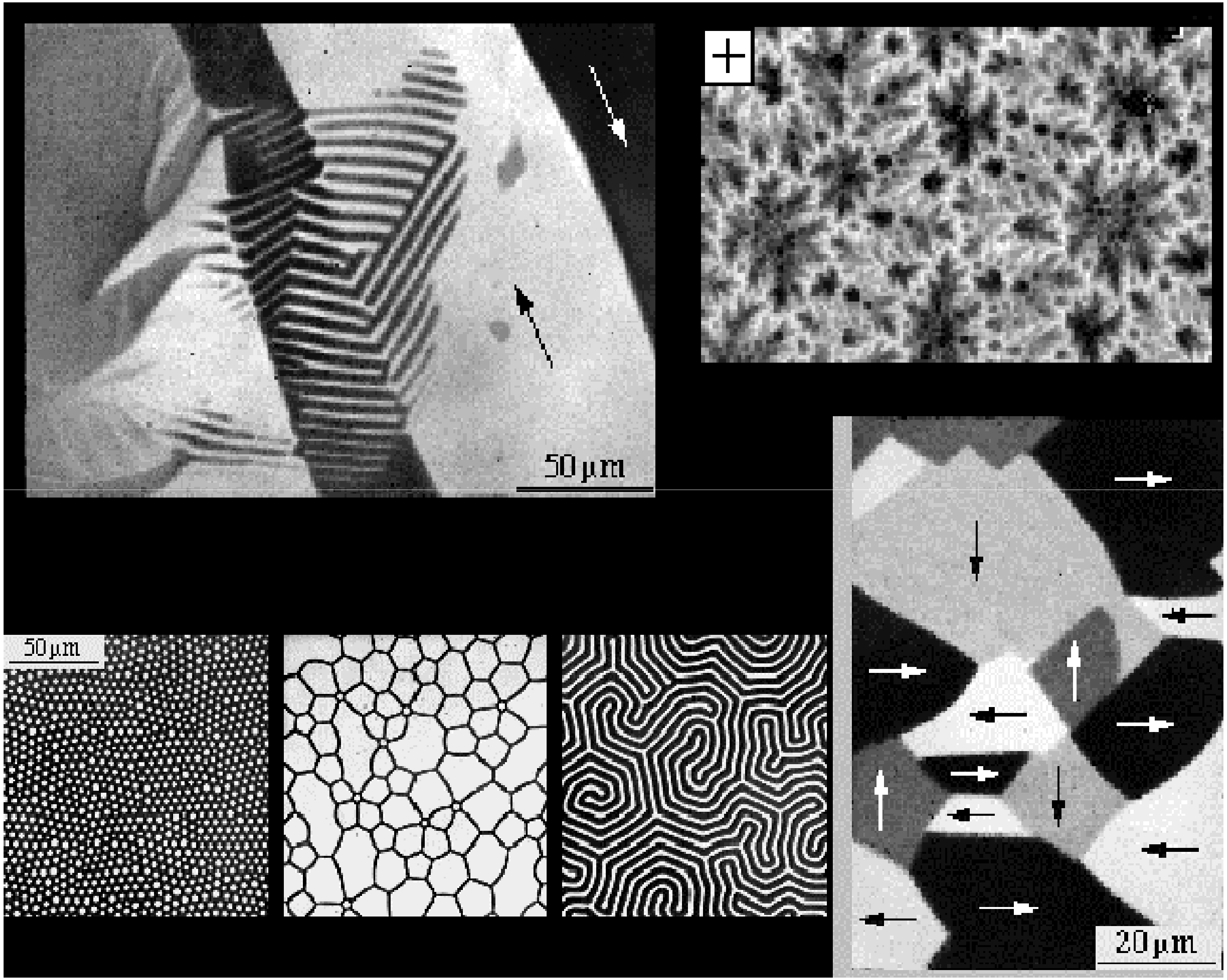

50 μm
50 μm
20 μm

X-ray, Neutron and Other Methods

Fig. 2.48b X-ray topography displays 90° domain walls and dislocations in a silicon iron sheet at the same time (Courtesy *J. Miltat*)

http://www.ifw-dresden.de/~schaefer/ToCBilder/2.7.htm

Comparison of Domain Observation Methods

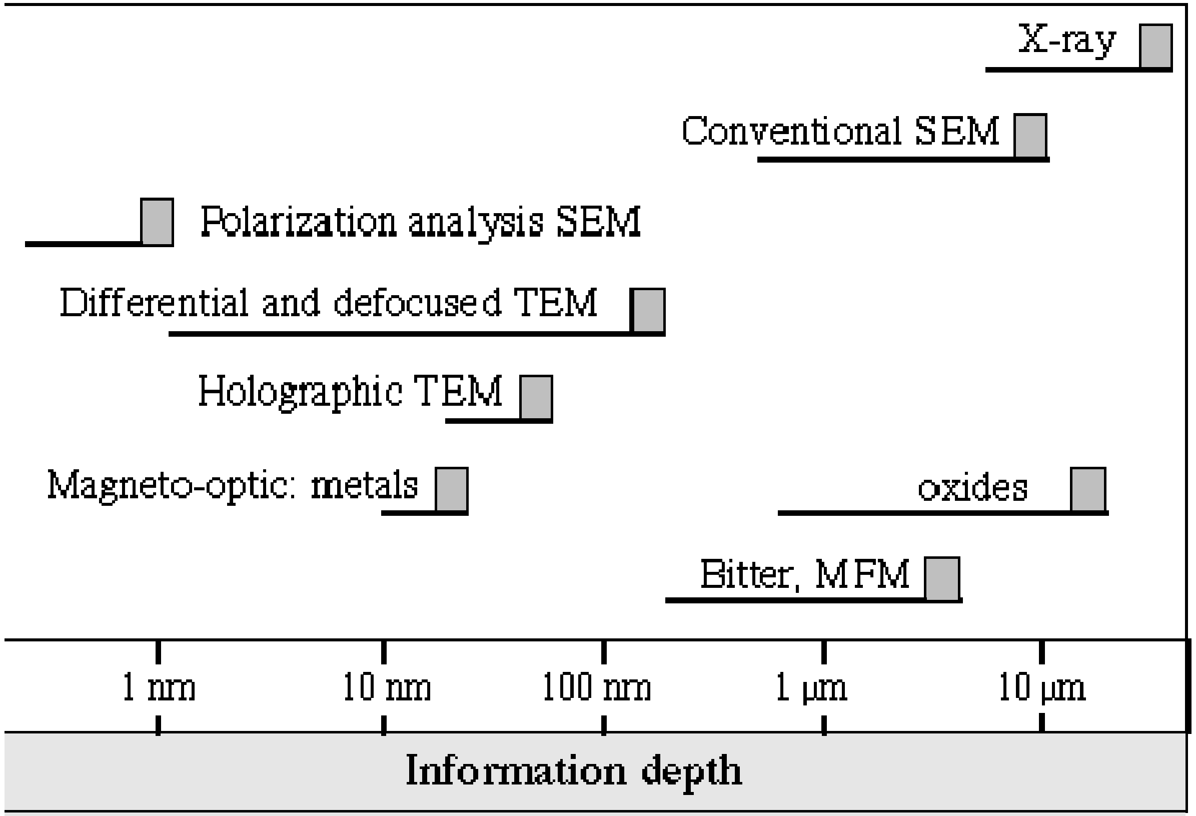

One of several criteria used in the comparison of domain observation techniques. SEM = Scanning (reflection) electron microscopy, TEM = transmission electron microscopy, MFM = magnetic force microscopy